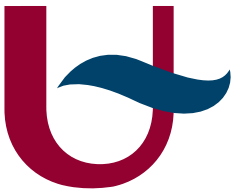

UNIVERSITEIT ANTWERPEN

Faculteit Wetenschappen

Departement Fysica

Numerical Simulation of the Electrical Response of a Ballistic Hall Bar in the Presence of an Inhomogeneous Magnetic Field Profile

Eindverhandeling ingediend tot het bekomen van de meestergraad
nanofysica

Yunlai Hao

Promotor: Prof. dr. François Peeters
Co-promotor: Dr. Ben Baelus

Academiejaar 2005-2006
Antwerpen

致我的父母

To my parents

ACKNOWLEDGMENTS

I would like to start this thesis with a word of tribute to those people who have greatly helped me on my work.

My great thanks to Prof. Dr. François Peeters who has accepted to be the Promotor of my advanced master thesis, prepared me such an interesting research topic and provided me with constant support, excellent and invaluable guidance and for his great patience to read and correct my thesis. With his advices and encouragement which have made it possible to attain the present form of this thesis. During my study, it has been an important and wonderful experience for me to take a place in his distinguished research group under his supervision.

I also would like to express my deep gratitude to my co-promotor Dr. Ben Baelus for his patience to help me in solving some of the computer program problems and for his providing me some nice materials which are greatly helpful for my work.

My thanks also go to my classmates Ben Xu and Dong Sun for their helpful suggests and discussions. The PhD-candidates An and Yosyp also help me a lot, I thank them for their help in answering my academic questions and in solving many problems regarding software application.

Furthermore, I strongly feel the necessity to thank all the Professors who have given me class during my study at University Antwerp, for their valuable instruction, helpful advice and critical evaluation.

Yunlai Hao
Antwerpen-2006

Contents

1 Introduction

1.1 HALL EFFECT

The Hall effect refers to the phenomena that when a magnetic field applied perpendicular to a thin sheet of conducting or semiconducting material in the form of a 'Hall bar' through which an electric current is flowing, one will find a potential difference (Hall voltage) on the opposite sides of the Hall bar due to the deflection of the charge carriers by the Lorentz force (see Fig. 1.1). Edwin Hall discovered this effect in 1879[1].

The Hall resistance is usually used to describe the Hall effect, it is defined as the Hall voltage divided by the amount of current in the Hall bar. Another important parameter for the Hall effect is the Hall coefficient, which is defined as the product of the Hall resistance and the Hall bar's thickness divided by the magnetic field, and it is a characteristic of the material of which the Hall bar is composed.

One very important feature of the Hall effect is that it differentiates between positive charges moving in one direction and negative charges moving in the opposite. The Hall effect offered the first real proof that electric currents in metals are carried by moving electrons, not by protons. The Hall effect also showed that in some substances (especially semiconductors), it is more appropriate to think of the current as positive 'holes' moving rather than negative electrons. On the other hand, by measuring the Hall voltage across the Hall bar, one can determine the strength of the magnetic field applied.

In the presence of high magnetic field strength and low temperature, one can observe the quantum Hall effect[2] in a two-dimensional electron gas

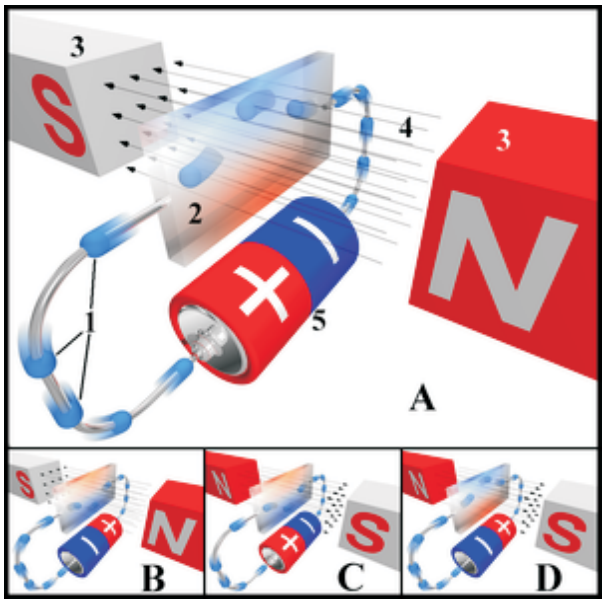

Fig. 1.1 Hall effect diagram, showing electron flow (rather than conventional current). Legend: 1. Electrons 2. Hall bar, or Hall sensor 3. Magnets 4. Magnetic field 5. Power source. Description: (A) the Hall bar takes on a negative charge at the top edge (blue color) and positive at the lower edge (red color). In (B) and (C), either the electric current or the magnetic field is reversed, causing the polarization to reverse. (D) Reversing both current and magnetic field causes the Hall element to again assume a negative charge at the upper edge.

(2DEG) systems, which is the quantization of the Hall resistance due to fundamental new physical properties of the 2DEG in high magnetic fields.

1.2 HALL EFFECT SENSORS

The features of the Hall effect make it very suitable to be utilized in various sensors. Actually, so-called "Hall effect sensors" are readily available from a number of different manufacturers, such as fluid flow sensors, power sensors, and pressure sensors. Hall effect devices produce a very low signal level and thus require amplification. While suitable for laboratory instruments, the vacuum tube amplifiers available in the first half of the 20th century were too expensive, power consuming, and unreliable for everyday applications. It was only with the development of the low cost integrated circuit (IC) that the Hall effect sensor became suitable for mass applications. A typical Hall effect sensor in fact is a device containing both a Hall sensor and a high gain IC amplifier in a single package.

Advantages: Hall effect devices when appropriately packaged are immune to dust, dirt, mud, and water. These characteristics make Hall effect devices better for position sensing than alternative means such as optical and electromechanical sensing.

When electrons flow through a conductor, a magnetic field is produced. Thus, it is possible to create a non-contacting current sensor. This has several advantages: no additional resistance need be inserted in the primary circuit. Also, the voltage present on the line to be sensed is not transmitted to the sensor, which enhances the safety of measuring equipment.

For example, we can use the Hall effect of a known 2DEG as a probe for the magnetic field. Such Hall probe has the following advantages: (1) noninvasive nature, (2) their high magnetic field sensitivity, (3) their very small active region, which by using modern microfabrication techniques can be of submicron dimensions, and (4) their broad temperature and magnetic field region over which they can be used. The scanning Hall probe microscope (SHPM) is a sensitive instrument which use a Hall probe to obtain quantitative measurements of surface magnetic field profiles with high spatial resolution ($\leq 1\mu$m)[3].

1.3 THE AIM OF THIS THESIS

In this thesis, We will investigate the response of a micron-sized Hall bar in the presence of a strong inhomogeneous magnetic field which is created by different type of ferromagnetic 'dots'. The latter can be magnetized cylinders, boxes or thin-films (see Fig.1.2). The position of these dots is arbitrary, resulting in a magnetic field with a complicate profile. We will discuss how to calculate the magnetic field profile for these dots in chapter **3**. The electrons moving inside the Hall bar are assume to be in the ballistic regime, which is applicable at low temperature (up to liquid nitrogen temperatures). At this regime, the mean free path of electrons is much longer than the geometry of the Hall bar, so the electrons will not experience scattering and will only be reflected at the boundaries. A billiard-ball model for the electron transport in this regime is adopted to simulate the electrons' trajectories, the transport probabilities of electrons can be obtained from this simulation, which will be used in the Landauer-Büttiker formula. The Hall resistance and bend resistance then follow from this formula. The details of this model will be discussed in chapter **2**. And in chapter **4** and **5**, We will discuss the results of our simulation for different geometries of magnetic dots and double dots.

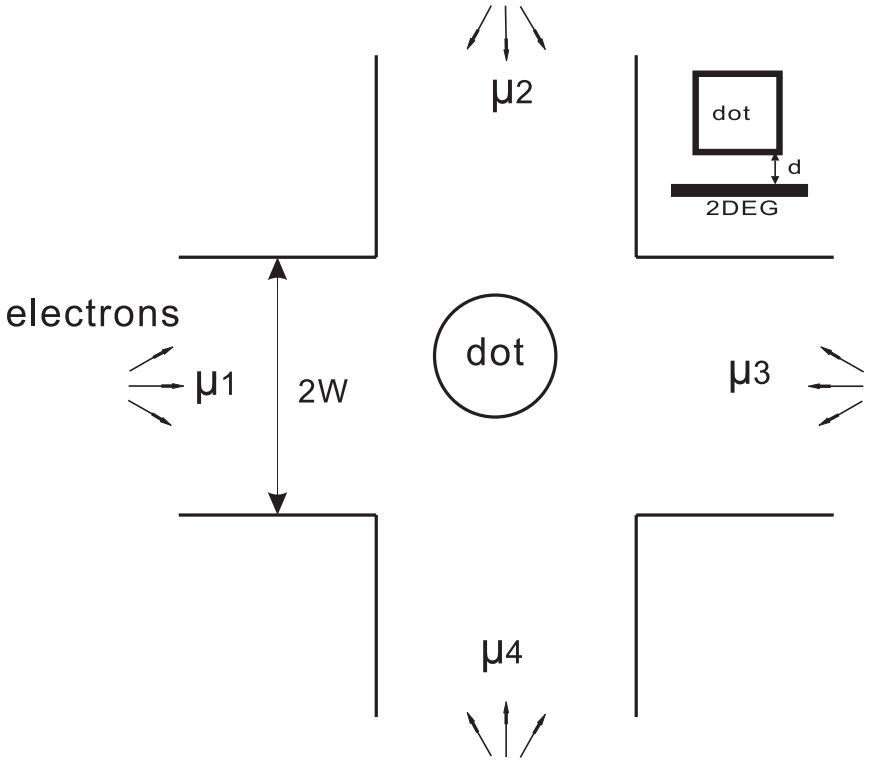

Fig. 1.2 The configuration of the systems to be investigated: Ballistic electrons are injected into a Hall cross in the presence of some ferromagnetic dots which put on top of the 2DEG. Top right inset: the distance between the dots and the 2DEG is d.

2

Landauer-Büttiker Formalism

The Landauer-Büttiker (LB) scattering approach is nowadays almost exclusively used for computing the conductance g for many materials in nanoscience. This very appealing formalism is particularly suitable for small systems, whose scale reach down to a few micrometers [4],[5]. Generally, at these systems, classical drift-diffusion models have limited success. The system we want to investigate in this thesis is a micron-sized Hall bar in the presence of an inhomogeneous magnetic field, where electrons at ballistic regime are injected into it. We shall see, that the Hall resistance and bend resistance of such a system can be deduced from the Landauer-Büttiker formulae.

2.1 BASIC CONCEPTS

Let's consider a resistor as a conductor sandwiched between two contacts, see Fig.2.1. From Ohm's law, we know, that the resistance can be expressed by a specific, material dependent but geometry independent resistivity ρ, or, equivalently, its conductivity σ, as:

$$R_0 = G_0^{-1} = \frac{L}{\sigma W}. \tag{2.1}$$

From this equation, if we tend the geometry to zero, the resistance also goes zero:

$$\lim_{L \to 0} R_0 = 0 \quad \text{(wrong)}. \tag{2.2}$$

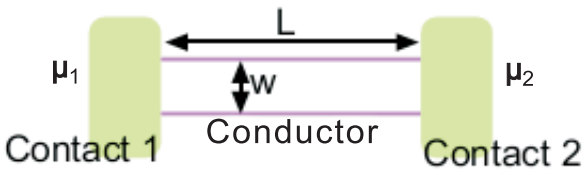

Fig. 2.1 A conductor sandwiched between two contacts

But this is not observed experimentally. For the length L going to zero and for small width W, we find a limiting value $\lim_{L\to 0} = R_C(W)$, which does depend on the width. To find an explanation, we introduce several concepts [6].

2.1.1 Transport probability

Conductance should be related to the ease with which electrons can pass, so we can introduce *the transmission probability* T as the probability for an electron to transmit through the conductor. Certainly, the reflection probability will be given by $1 - T$. A ballistic conductor is an ideal transmitting conductor without scatterers, having a transmission probability of $T = 1$.

2.1.2 Transverse modes

As we will see, electronic transport happens in discrete channels through a narrow conductor, which we call transverse modes. The electron dynamics in effective mass approximation inside the conductor is described by Schrödinger equation:

$$\left[E_C + \frac{p^2}{2m^*} + V(x,y)\right]\psi(x,y,z) = E\psi(x,y,z). \tag{2.3}$$

Here, E_C is the conduction band edge of the conductor material and $V(x,y)$ is a confining potential. Since the system confining potential is translational invariant in the z direction, we choose a separating ansatz $\psi(x,y,z) = \chi(x,y)\exp(ik_z z)$, which yields:

$$\begin{cases} \left[\frac{p_x^2+p_y^2}{2m^*} + V(x,y)\right]\chi_n(x,y) = \varepsilon_n\chi_n(x,y), \\ \\ E_n(k_z) = E_C + \frac{\hbar^2 k_z^2}{2m^*} + \varepsilon_n. \end{cases} \tag{2.4}$$

The $\chi_n(x,y)$ are called transverse modes and n is an index for the discrete spectrum. With this we can find that the contacts look to be reflectionless: An electron inside the conductor most probably will find an empty state in the contact when exiting, for we have almost infinitely many modes in a wide

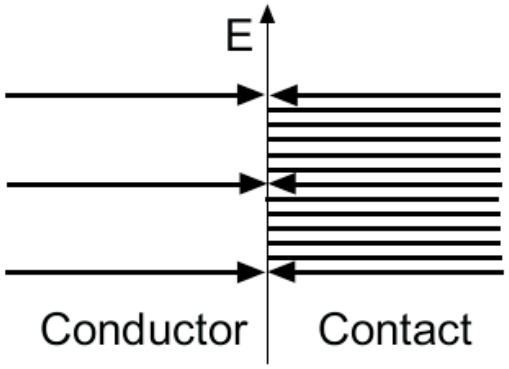

Fig. 2.2 States in a conductor and contact

contact. For an electron in the contact, however, we have a different situation: To enter the conductor it must have exactly the correct energy corresponding to an empty transverse mode. Fig. 2.2 illustrates this matter. From now on we simply use k instead of k_z.

2.2 LANDAUER FORMULA

For a ballistic conductor sandwiched between two contacts whose electrochemical potentials are μ_1 and μ_2 respectively (see Fig. 2.1) its transverse modes are shown in Fig. 2.3. At low temperature, normally we can take:

$$\begin{aligned} \mu_1 &= \mu = E_F, \\ \mu_2 &= \mu + \delta\mu. \end{aligned} \tag{2.5}$$

The net current carried by state(or mode) n will be:

$$\begin{aligned} j_n &= ev_n N_n \\ &= \tfrac{1}{2} ev_n \textstyle\int_{E_F}^{E_F+\delta\mu} D_n(E)dE. \end{aligned} \tag{2.6}$$

The coefficient $\frac{1}{2}$ comes from the fact that only $v_n > 0$ electrons contribute to the current.

$$\text{from:} \quad \left.\begin{aligned} E_n &= \tfrac{mv_n^2}{2} \\ mv_n &= \hbar k \end{aligned}\right\} \Rightarrow v_n = \frac{1}{\hbar}\frac{dE_n}{dk}. \tag{2.7}$$

In 1D electron gas, $D(E) = \frac{1}{\pi\hbar}\sqrt{\frac{2m}{E}}$, with Eq. (2.7), one gets:

$$D_n(E) = \frac{2}{\pi \frac{dE_n}{dk}}. \tag{2.8}$$

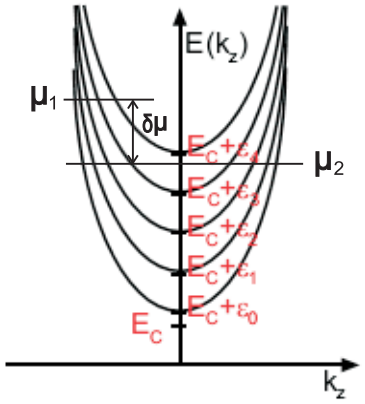

Fig. 2.3 Schematic dispersion relations for some transverse modes

Substitute Eq. (2.7) and Eq. (2.8) into Eq. (2.6), we have:

$$j_n = e\int_{E_F}^{E_F+\delta\mu} dE \frac{1}{\hbar}\frac{dE_n}{dk}\frac{1}{2}\frac{2}{\pi\frac{dE_n}{dk}} = \frac{2e}{h}\delta\mu. \tag{2.9}$$

Here $\frac{2e}{h} = 80\frac{nA}{meV}$is the current per state per energy. The total current will be a sum over all the states:

$$j_{total} = \sum_{n=1}^{N} j_n = N\frac{2e}{h}\delta\mu. \tag{2.10}$$

The voltage we applied here is $V = \frac{\delta\mu}{e}$, so the conductance will be:

$$G = \frac{2e^2}{h}N. \tag{2.11}$$

and the resistance(contact resistance) is:

$$R_C = \frac{h}{2e^2N} \approx \frac{12.9\text{k}\Omega}{N}. \tag{2.12}$$

These results have been confirmed experimentally, see Fig. 2.4.

A fully analogous treatment including resident scatterers inside the conductor yield:

$$I = \frac{2e}{h}\sum_{n=1}^{N} T_n\delta\mu. \tag{2.13}$$

Where T_n is the transmission probability for mode n. With $V = \frac{\delta\mu}{e}$, we get Landauer's formula[8] for the conductance of a mesoscopic conductor:

$$G = \frac{2e^2}{h}\sum_{n=1}^{N} T_n. \tag{2.14}$$

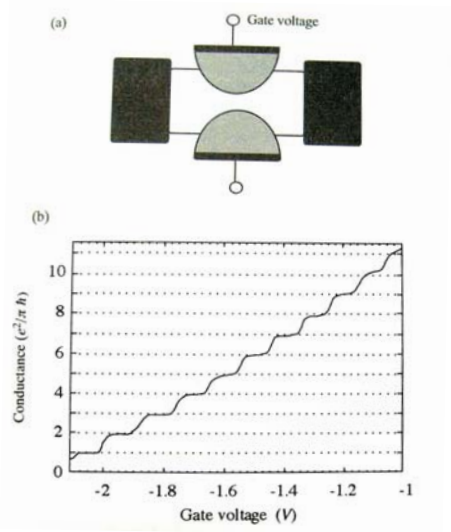

Fig. 2.4 Quantized conductance of a ballistic waveguide. (a) A negative voltage on a pair of metallic gates (called the split-gate configuration) is used to deplete and narrow down the constriction progressively. (b) Measured conductance vs. gate voltage. [7]

2.3 MULTI-TERMINAL DEVICES, BÜTTIKER'S FORMULA

Now we want to extend our investigations to multi-terminal devices[9], having more than 2 probes (see Fig. 2.5). We can introduce a fifth chemical potential μ_0 below which all electron states are occupied everywhere and cannot contribute to the current. For probe i, From Eq. (2.10):

$$I = N_i \frac{2e}{h}(\mu_i - \mu_0). \tag{2.15}$$

A quantum form of Kirchhoff's current laws gives the desired result. Of the current incident into probe i, a fraction R_{ii} is reflected and the net inward current is further reduced by those currents incident from other probes that transmit out of probe i. Thus

$$I_i = \frac{2e}{h}[(N_i - R^*_{ii})(\mu_i - \mu_0) - \sum_{j \neq i} T^*_{ij}(\mu_j - \mu_o)]. \tag{2.16}$$

Where R^*_{ii} and T^*_{ij} are the reflection and transport coefficient respectively, they represent the total probability of reflection at probe i or transport form probe $i \to j$, and are given by a sum over all occupied modes (indices k, l) in both probes: $R^*_{ii} = \sum_{kl} R_{ii,kl}$, $T^*_{ij} = \sum_{kl} T_{ij,kl}$. From the current conservation for probe i:

$$N_i = R^*_{ii} + \sum_{j \neq i} T^*_{ij}. \tag{2.17}$$

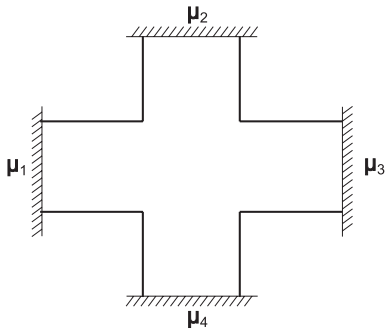

Fig. 2.5 The four terminal device for Landauer-Büttiker formula

Substitute this into Eq. (2.16), one gets:

$$I_i = \frac{2e}{h} \sum_{j \neq i} T_{ij}^* (\mu_i - \mu_j). \tag{2.18}$$

Then the four-terminal resistance[10], where the voltage $V_{kl} = (\mu_k - \mu_l)/e$ is measured between terminals k and l while the current goes from m to n, is

$$R_{mn,kl} = \frac{h}{2e^2} \frac{T_{km}^* T_{ln}^* - T_{kn}^* T_{lm}^*}{D_{ml}^*}. \tag{2.19}$$

Where D_{ml}^* is the subdeterminant of the matrix of all the transport coefficients (this matrix can be determined by experiment, see Ref.[11]) but with row m and column n deleted. For the Hall cross we used in this thesis with four identical probes, we have $N_i \equiv N$ and $T_{ij}^* \equiv N T_{ij}$, where T_{ij} is the transport probability for the electrons go from probe i to probe j, thus yields:

$$R_{mn,kl} = N \frac{h}{2e^2} \frac{T_{km} T_{ln} - T_{kn} T_{lm}}{D_{ml}}. \tag{2.20}$$

2.4 SEMICLASSICAL BILLIARD MODEL OF BALLISTIC ELECTRONS

To obtain the transport probabilities for the electrons moving inside a Hall cross at ballistic regime, we simulate the motion of the electrons using a semiclassical billiard model[12].

2.4.1 Initial condition

A large number of electrons(typically 10^6 for each probe) are injected from all four probes with an initial velocity $v = v_F = \sqrt{2mE_F}$. We follow its

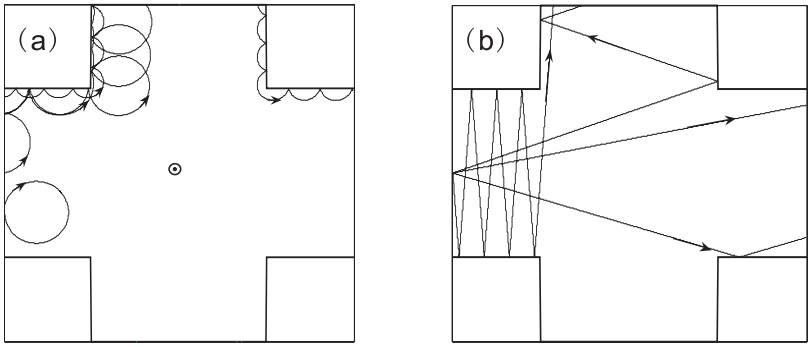

Fig. 2.6 Typical electron trajectories in Hall cross: (a) with uniform external magnetic field; (b) no external field present.

trajectories (see Fig. 2.6) to determine the number of electrons leaving via probe j as t_{ij}, and the number of electrons that are reflected, as r_{ii}. The electrons are injected from one probe at different positions and different angels. If we use a random generator to do this, there are too much electrons needed. Instead, like a perfect random generator, we inject equal amount of electrons at every position along the lead boundary, with the angular distribution $P(\alpha) = \frac{1}{2}\cos\alpha$, with α the injection angle, $\alpha \in (-\pi/2, \pi/2)$. Actually the largest injection angel should be a little less than $\pi/2$, since a too high injection angel has no meaning here. So, considering the angular distribution, we have:

$$t_{ij} = \sum_{\text{all e: } i\to j} P(\alpha), \quad \text{(sum over all electrons from lead } i \text{ to lead } j\text{)}$$
$$r_{ii} = \sum_{\text{all e: } i\to i} P(\alpha). \tag{2.21}$$

Finally the transport probability will be:

$$T_{ij} = \frac{t_{ij}}{r_{ii} + \sum_{k\neq i} t_{ik}}. \tag{2.22}$$

2.4.2 Transport mechanism

The motion of a ballistic electron is determined by Newton's equation:

$$x_i = x_{i0} + v_{ix}\cdot dt + \frac{1}{2}a_{ix}\cdot dt^2,$$
$$y_i = y_{i0} + v_{iy}\cdot dt + \frac{1}{2}a_{iy}\cdot dt^2. \tag{2.23}$$

with (v_{ix}, a_{ix}) and (v_{iy}, a_{iy}) the velocity and acceleration in the x and y direction respectively. When an external magnetic field B applied (the direction of magnetic field shown in Fig.2.6), the electrons will be driven by the Lorentz force, we have:

$$ma_{ix} = -eB \cdot v_{iy},$$
$$ma_{iy} = eB \cdot v_{ix}.$$

where e is the electron charge and m is the effective mass for electrons move in 2DEG.

Reflection in the leads:

Like a classical rigid ball, a ballistic electron will be specular reflected when it hits a wall.

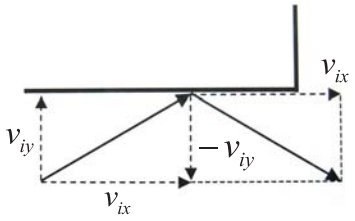

Fig. 2.7 Reflection at lead boundary

Reflection at rounded corner:

When we have a Hall cross with rounded corners, the situation become a little more complicated (see Fig. 2.8). The reflection angle is the sum of a simple reflection and a rotation as indicated in the figure:

$$\begin{pmatrix} v_{ix} \\ v_{iy} \end{pmatrix}_{\text{after a simple reflection}} = \begin{pmatrix} 1 & 0 \\ 0 & -1 \end{pmatrix} \begin{pmatrix} v_{ix} \\ v_{iy} \end{pmatrix} = \begin{pmatrix} v_{ix} \\ -v_{iy} \end{pmatrix},$$

$$\begin{pmatrix} v_{ix} \\ v_{iy} \end{pmatrix}_{\text{after rotation}} = \begin{pmatrix} \cos\alpha & -\sin\alpha \\ \sin\alpha & \cos\alpha \end{pmatrix} \begin{pmatrix} v_{ix} \\ v_{iy} \end{pmatrix}.$$

So, after the reflection at rounded corner:

$$\begin{aligned} \begin{pmatrix} v_{ix} \\ v_{iy} \end{pmatrix} &= \begin{pmatrix} \cos\alpha & -\sin\alpha \\ \sin\alpha & \cos\alpha \end{pmatrix} \begin{pmatrix} v_{ix} \\ -v_{iy} \end{pmatrix} \\ &= \begin{pmatrix} \cos\alpha \cdot v_{ix} + \sin\alpha \cdot v_{iy} \\ \sin\alpha \cdot v_{ix} - \cos\alpha \cdot v_{iy} \end{pmatrix}. \end{aligned} \tag{2.24}$$

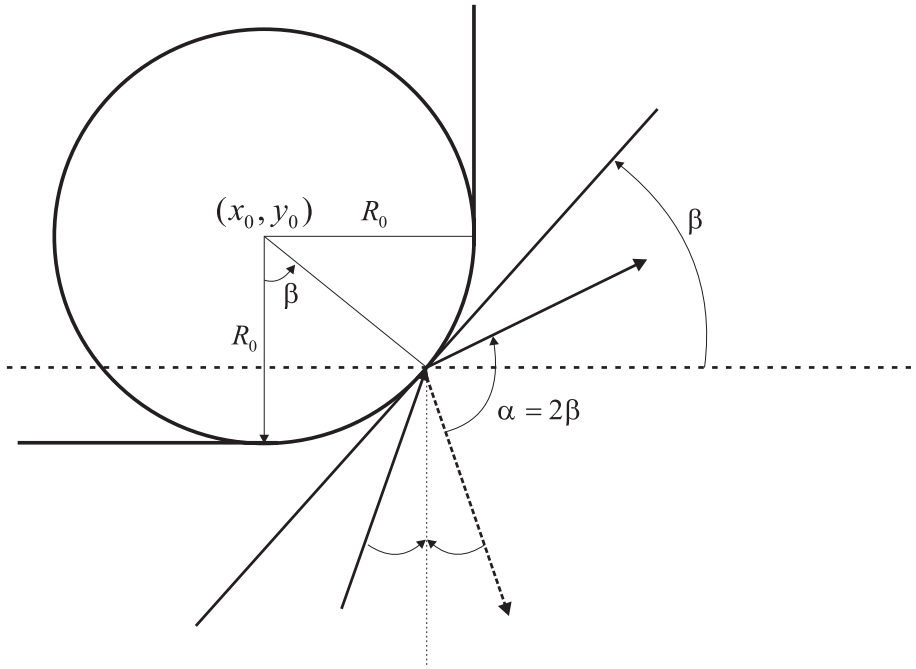

Fig. 2.8 Reflection at rounded corner

2.5 THE TRANSPORT PROBABILITIES FOR A HALL CROSS WITH UNIFORM EXTERNAL FIELD

Using the method mentioned above, the transport probabilities of a Hall cross with uniform external field were calculated (see Fig. 2.9). The electron density is set to $n_e = 3.45 \times 10^{15}\, m^{-2}$, and the width of the lead of the Hall cross is $2W = 1.85\, \mu m$, in accordance with Ref.[4]. We can see that the reflection always increases when the strength of magnetic field increases, this is reasonable since the cyclotron diameter decreases with magnetic field, and the small cyclotron diameter makes an electron easier to leave from the same lead where it has been injected, like in Fig. 2.6(a). For the same reason, T_{13} very rapid goes to zero when the magnetic field increases to about 0.11 T. T_{12} and T_{14} will also go to zero when the magnetic field with the right direction which turns electrons away from lead 2 or lead 4 respectively, but at a smaller field strength compared to T_{13}: 0.08T for T_{12} and -0.08T for T_{14}. The peak of T_{12} and T_{14} happened at about 0.096 T.

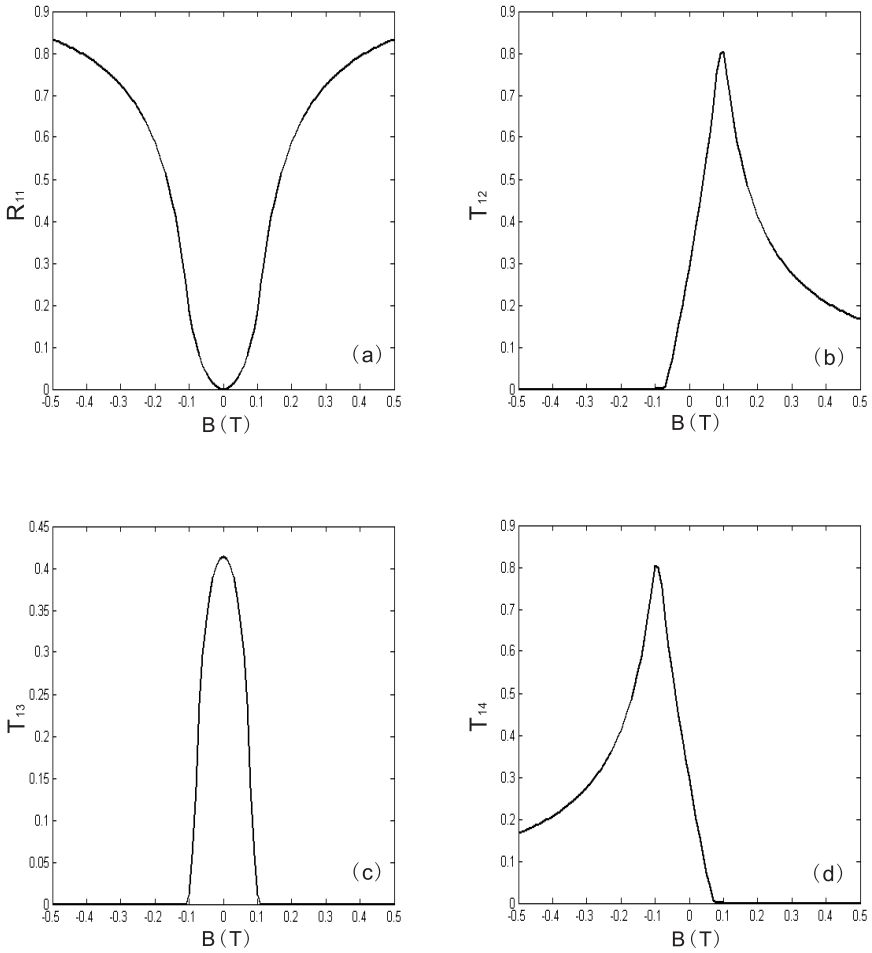

Fig. 2.9 Transport probabilities for a hall cross with uniform external magnetic field. (a). R_{11} vs. B (b). T_{12} vs. B (c). T_{13} vs. B (d). T_{14} vs. B.

3

Magnetic Field Profile

In this chapter, we discuss how to calculate the magnetic field profile of a ferromagnetic cylinder, box and thin film. The magnetic field profile will be used in the further simulation.

3.1 MAGNETIZED BOX AND FILM

The configuration of our magnetized box and film is shown in Fig.3.1. For a box with a uniform magnetization M_z along z direction, we will calculate the the magnetic field at z direction, since our electrons move in a plane vertical to z axis and only the magnetic field in z direction is effective. For the film, actually we can treat it as a very thin box, but with a magnetization along x direction. The scalar potential of a magnetized box is[13]:

$$\Phi_m(\vec{r}) = -\frac{1}{4\pi}\int_V \frac{\nabla' \cdot \vec{M}(\vec{r'})}{|\vec{r}-\vec{r'}|}d^3\vec{r'} + \frac{1}{4\pi}\oint_S \frac{\vec{n}' \cdot \vec{M}(\vec{r'})}{|\vec{r}-\vec{r'}|}dS'. \tag{3.1}$$

Thanks to the uniform magnetization M_z, the first term of Eq. (3.1) vanishes:

$$\Phi_m(\vec{r}) = \frac{1}{4\pi}\oint_S \frac{\vec{n}' \cdot \vec{M}(\vec{r'})}{|\vec{r}-\vec{r'}|}dS', \tag{3.2}$$

$$= -\frac{1}{4\pi}\int_{S_1} \frac{M_z dx'dy'}{\sqrt{(x-x')^2+(y-y')^2+(z-z_1)^2}} + \frac{1}{4\pi}\int_{S_2} \frac{M_z dx'dy'}{\sqrt{(x-x')^2+(y-y')^2+(z-z_2)^2}}. \tag{3.3}$$

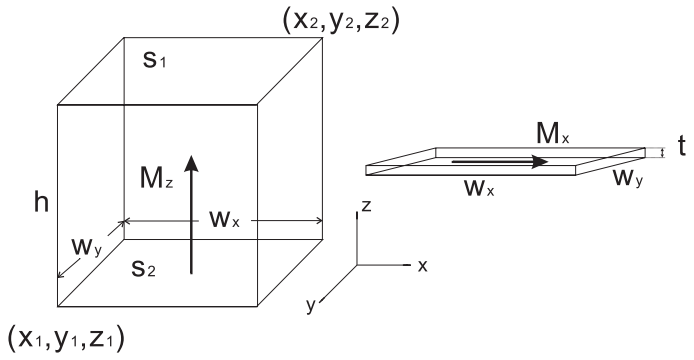

Fig. 3.1 The configuration for magnetized box and thin film.

The relation of the scalar potential Φ_m and magnetic induction field $\vec{B}$ is:

$$\vec{B} = -\mu_0 \nabla \Phi_m. \tag{3.4}$$

Since we want to calculate the magnetic field in z direction, from Eq. (3.3) and Eq. (3.4), one get:

$$\begin{aligned} B_z &= -\mu_0 \frac{\partial \Phi_m}{\partial z}, & (3.5)\\ &= -\frac{\mu_0 M_z}{4\pi} \int_{S1} \frac{(z-z_1)dx'dy'}{[(x-x')^2+(y-y')^2+(z-z_1)^2]^{3/2}} \\ &\quad +\frac{\mu_0 M_z}{4\pi} \int_{S2} \frac{(z-z_2)dx'dy'}{[(x-x')^2+(y-y')^2+(z-z_2)^2]^{3/2}}. & (3.6) \end{aligned}$$

From Eq. (3.6), we need to integrate in the top surface S_1, and the bottom surface S_2 of the box, first we integrate by x':

$$\begin{aligned} B_z = &-\frac{\mu_0 M_z}{4\pi} \int \frac{(z-z_1)(x_2-x)dy'}{[(y-y')^2+(z-z_1)^2]\sqrt{(x-x_2)^2+(y-y')^2+(z-z_1)^2}} \\ &+\frac{\mu_0 M_z}{4\pi} \int \frac{(z-z_1)(x_1-x)dy'}{[(y-y')^2+(z-z_1)^2]\sqrt{(x-x_1)^2+(y-y')^2+(z-z_1)^2}} \\ &+\frac{\mu_0 M_z}{4\pi} \int \frac{(z-z_2)(x_2-x)dy'}{[(y-y')^2+(z-z_2)^2]\sqrt{(x-x_2)^2+(y-y')^2+(z-z_2)^2}} \\ &-\frac{\mu_0 M_z}{4\pi} \int \frac{(z-z_2)(x_1-x)dy'}{[(y-y')^2+(z-z_2)^2]\sqrt{(x-x_1)^2+(y-y')^2+(z-z_2)^2}}. \end{aligned} \tag{3.7}$$

Then we integrate by y', finally we have our expression of the magnetic field as:

$$\begin{aligned} B_z &= -f_{x_2y_2z_1} + f_{x_2y_1z_1} + f_{x_1y_2z_1} - f_{x_1y_1z_1} \\ &\quad +f_{x_2y_2z_2} - f_{x_2y_1z_2} - f_{x_1y_2z_2} + f_{x_1y_1z_2}, & (3.8) \end{aligned}$$

where:

$$f_{\alpha\beta\gamma} = \frac{\mu_0 M_z}{4\pi} \arctan\left[\frac{(\alpha - x)(\beta - y)}{(z-\gamma)\sqrt{(\alpha - x)^2 + (\beta - y)^2 + (\gamma - z)^2}}\right]. \quad (3.9)$$

In Fig.3.4, we show some typical magnetic field profile for magnetized boxes.

Now we calculate B_z for the magnetized films, actually we can treat them as a very thin box with the magnetization in x direction, alternatively, they are the same to the z magnetized boxes' magnetic field in x direction, from Eq. (3.4):

$$B_x = -\mu_0 \frac{\partial \Phi_m}{\partial x}, \quad (3.10)$$

substitute this into Eq. (3.3):

$$\begin{aligned} B_x &= -\frac{\mu_0 M_z}{4\pi} \int_{S1} \frac{(x - x')dx'dy'}{[(x-x')^2 + (y-y')^2 + (z-z_1)^2]^{3/2}} \\ &\quad + \frac{\mu_0 M_z}{4\pi} \int_{S2} \frac{(x - x')dx'dy'}{[(x-x')^2 + (y-y')^2 + (z-z_2)^2]^{3/2}}. \end{aligned} \quad (3.11)$$

Then, still, integrate this equation in surface S_1 and S_2, one gets:

$$\begin{aligned} B_x &= -g_{x_2y_2z_1} + g_{x_2y_1z_1} + g_{x_1y_2z_1} - g_{x_1y_1z_1} \\ &\quad + g_{x_2y_2z_2} - g_{x_2y_1z_2} - g_{x_1y_2z_2} + g_{x_1y_1z_2}, \end{aligned} \quad (3.12)$$

where:

$$g_{\alpha\beta\gamma} = \frac{\mu_0 M_z}{4\pi} \text{arcsinh}\left[\frac{(\beta - y)}{\sqrt{(\alpha - x)^2 + (\gamma - z)^2}}\right]. \quad (3.13)$$

The typical magnetic field of a magnetized film is shown in Fig. 3.3.

3.2 MAGNETIZED CYLINDER

For a magnetized cylinder, we can still calculate its magnetic field profile as we done to box, but the problem is that the integration in cylindrical coordinates involved complicated functions which make the solution also very complicate. Actually, for a cylinder we can utilize its high symmetry property, note that the cylinder has an azimuthal symmetried magnetic field profile, and for an azimuthal symmetry problem here, we have a general solution[13]:

$$\Phi(r, \theta) = \sum_{l=0}^{\infty} [A_l r^l + B_l r^{-(l+1)}] P_l(\cos\theta), \quad (3.14)$$

where:

$$\Phi(z = r) = \sum_{l=0}^{\infty} [A_l r^l + B_l r^{-(l+1)}]. \quad (3.15)$$

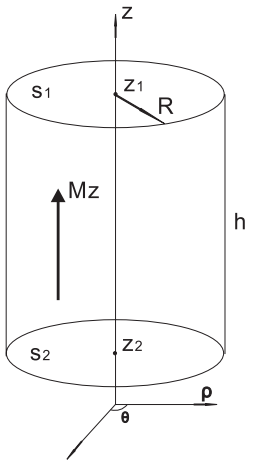

Fig. 3.2 The configuration for magnetized cylinder

is the solution for the problem at the symmetry axis, and $P_l(\cos\theta)$ is Legendre polynomials. So at first we just need to calculate B_z in the symmetry axis of the cylinder, from Eq. (3.6), integrate in s_1 and s_2, one gets:

$$B_z(z) = \frac{\mu_0 M_z}{2}[\frac{z-z_1}{\sqrt{R^2+(z-z_1)^2}} - \frac{z-z_2}{\sqrt{R^2+(z-z_2)^2}}]. \tag{3.16}$$

We need to expand it into power series, when $(z-z_1) \geq R$:

$$\begin{aligned} \frac{z-z_1}{\sqrt{R^2+(z-z_1)^2}} &= \frac{1}{\sqrt{\frac{R^2}{(z-z_1)^2}+1}} \\ &= \sum_{n=0}^{\infty} P_{2n}(0)\left(\frac{R}{z-z_1}\right)^{2n}; \end{aligned} \tag{3.17}$$

when $0 \leq (z-z_1) \leq R$:

$$\begin{aligned} \frac{z-z_1}{\sqrt{R^2+(z-z_1)^2}} &= \frac{\frac{z-z_1}{R}}{\sqrt{\left(\frac{z-z_1}{R}\right)^2+1}} \\ &= \sum_{n=0}^{\infty} P_{2n}(0)\left(\frac{z-z_1}{R}\right)^{2n+1}. \end{aligned} \tag{3.18}$$

Compare these two equations to the general solution Eq. (3.14), our magnetic field can be write as:

$$B_z = \frac{\mu_0 M_z}{2}[F(r_1,\theta_1) - F(r_2,\theta_2)], \tag{3.19}$$

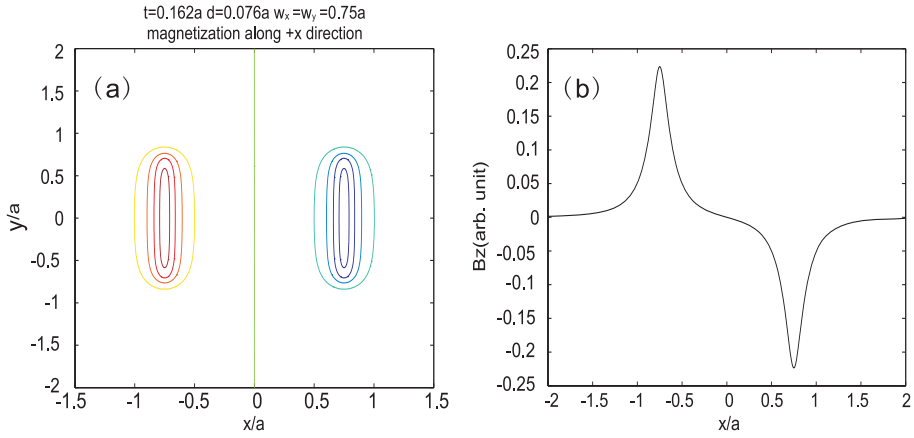

Fig. 3.3 Typical magnetic field for a magnetized film. The meaning of the symbol: a, is the unit for distance; t, thickness of the film; w_x and w_y, width of the film; d, the distance between the measure plane and the bottom surface of the film. (a) contour plot of B_z in a plane underneath the film; (b) The field strength along the x axis for a film using the same parameter as in (a).

where:

$$F(r_i,\theta_i) = \begin{cases} 1+\sum_{n=1}^{\infty} P_{2n}(0)\left(\frac{R}{r_i}\right)^{2n} P_{2n-1}(\cos\theta_i) & r_i \geq R \\ \sum_{n=0}^{\infty} P_{2n}(0)\left(\frac{r_i}{R}\right)^{2n+1} P_{2n+1}(\cos\theta_i) & 0 \leq r_i \leq R \end{cases} . \quad (3.20)$$

And $\cos\theta_i = \frac{z-z_i}{\sqrt{(z-z_i)^2+\rho^2}}$, $r_i = \sqrt{(z-z_i)^2+\rho^2}$, i is the index for the top surface S_1 and the bottom surface S_2.

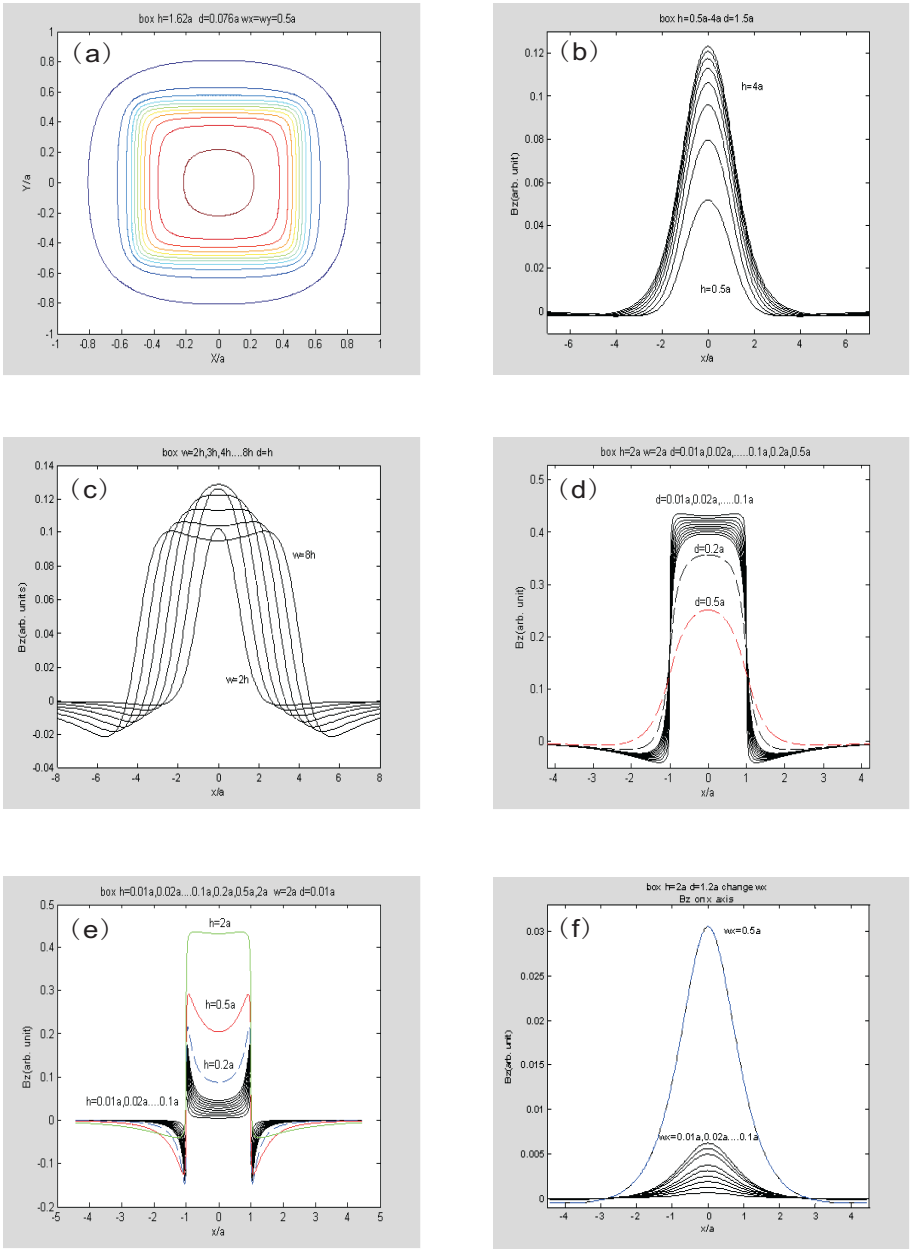

Fig. 3.4 Typical magnetic field for magnetized boxes. The meaning of the symbol: a, is the unit for distance; h, height of the box; w_x and w_y, width of the box; d, the distance between the measure plane and the bottom surface of the box. (a) contour plot of B_z in a plane underneath the box; (b) d and width hold, vary h; (c) d and h hold, vary width; (d)h and width hold, vary d; (e) d is very small, width hold, vary h; (f) d, h and w_y hold, vary w_x

4

Hall bar response in the presence of magnetized cylinders

The system under study is shown in Fig. 1.2. In this chapter, we discuss the situation that the inhomogeneous magnetic field is created by local magnetized cylinders. Hall resistance and bend resistance will be calculated and studied for different scenarios, the default parameters used for the calculation in this chapter is set to:
$n_e = 3.45 \times 10^{15}$ m^{-2}, the electron density for the 2DEG;
$V_F = \frac{\hbar\sqrt{2\pi n_e}}{m} = 2.54 \times 10^5$ m/s, the Fermi velocity, where $m = 0.067 m_e$ is the effective electron mass in GaAs;
$W = \frac{1.85}{2}$ μm $= 0.925$ μm, the half width of the lead in the Hall bar;
$h/W = 1.62$, the height of the dots;
$d/W = 0.076$, the distance between the dots and 2DEG;
$R/W = 0.81$, the radius of the cylinder dots.

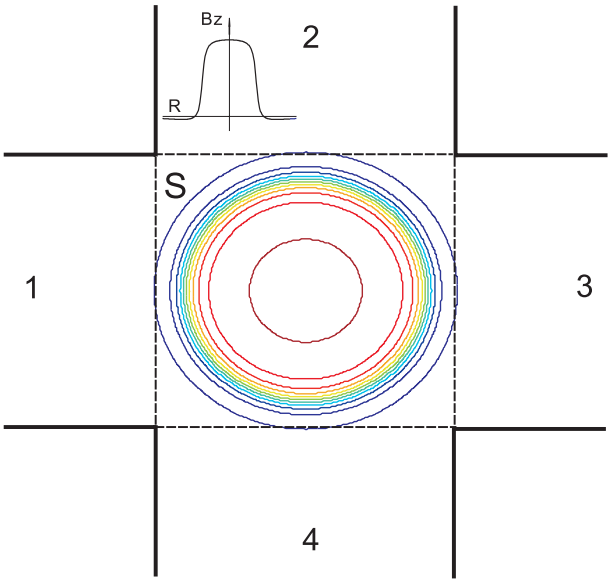

Fig. 4.1 Contour plot of magnetic field profile for a magnetized cylinder placed at the center of the Hall bar; S, the junction area. Top inset: the strength of magnetic field underneath the cylinder.

4.1 ONE CYLINDER

In this section, we discuss the scenario that there is only one magnetized cylinder placed in the Hall cross region. The typical magnetic field profile for such a cylinder is shown in Fig. 4.1.

4.1.1 One cylinder at the center of the Hall cross

First we put one cylinder at the center of the Hall cross, and vary its radius. With this configuration, in Fig. 4.2(a) we show the Hall resistance and in Fig. 4.2(b) the bend resistance as function of the average magnetic field in the junction area. The average magnetic field B_{av} is calculated by $B_{av} = \frac{\int_S B_z dS}{S}$, where S is the junction area of the Hall cross (dashed line square in Fig. 4.1). On the other hand, the magnetic field strength underneath the cylinder is also a very important parameter which actually determine how the electrons move in the junction, let B_{cen} indicate the field strength at the center of the area underneath the cylinder, for each particular cylinder, the relation between B_{av} and B_{cen} is determined only by the geometries. If we fix all the other parameters as default, for a $R/W = 0.4$ cylinder, B_{cen}=$8.18B_{av}$; $R/W = 0.7$, $B_{cen} = 2.78B_{av}$; $R/W = 1.0$, $B_{cen} = 1.37B_{av}$. In Fig.4.2 (c)

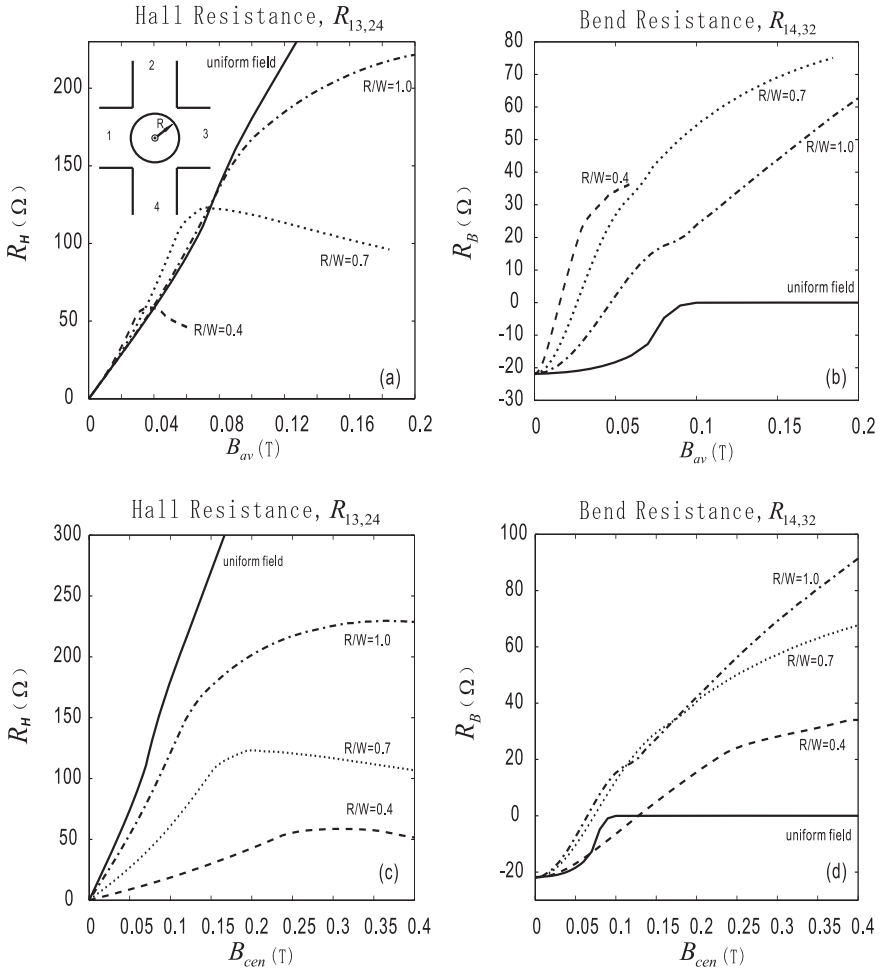

Fig. 4.2 The Hall resistances and bend resistances of a cylinder at center with different radius: (a) R_H vs. B_{av}. (b) R_B vs. B_{av}. (c) R_H vs. B_{cen}. (d) R_B vs. B_{cen}. Inset of (a): the configuration of the system.

and (d), we show the Hall resistance and the bend resistance as function of B_{cen}. When the strength of the magnetic field is low, from Ref.[14], we have the following equation:

$$\alpha = \frac{R_H}{B_{av}} = \text{Constant} \tag{4.1}$$

Which means the Hall factor α is simply depend on the average magnetic field B_{av} for any kind of practical magnetic field at low field strength condition. Our results here are in good agreement to this claim, as shown in Fig. 4.2(a)

for a magnetized cylinder at the center of the Hall cross with different radius. When B_{av} is not too large, the Hall resistances are identical to the one coming from a uniform magnetic field. Note that all the curves for a cylinder show very similar behavior when moving away from that of the uniform field one, they increase a little faster at intermediate field strength, then, a quick suppression at large field strength. To understand this increase then decrease behavior, we need to know what is the difference between a cylinder at the center of the Hall cross and a applied uniform external field for the transport probabilities. In Fig. 4.3, we plot the transport probabilities as function of B_{cen} for a $R/W = 0.7$ cylinder.
Compare these transport probabilities to those in Fig.2.9, one finds:

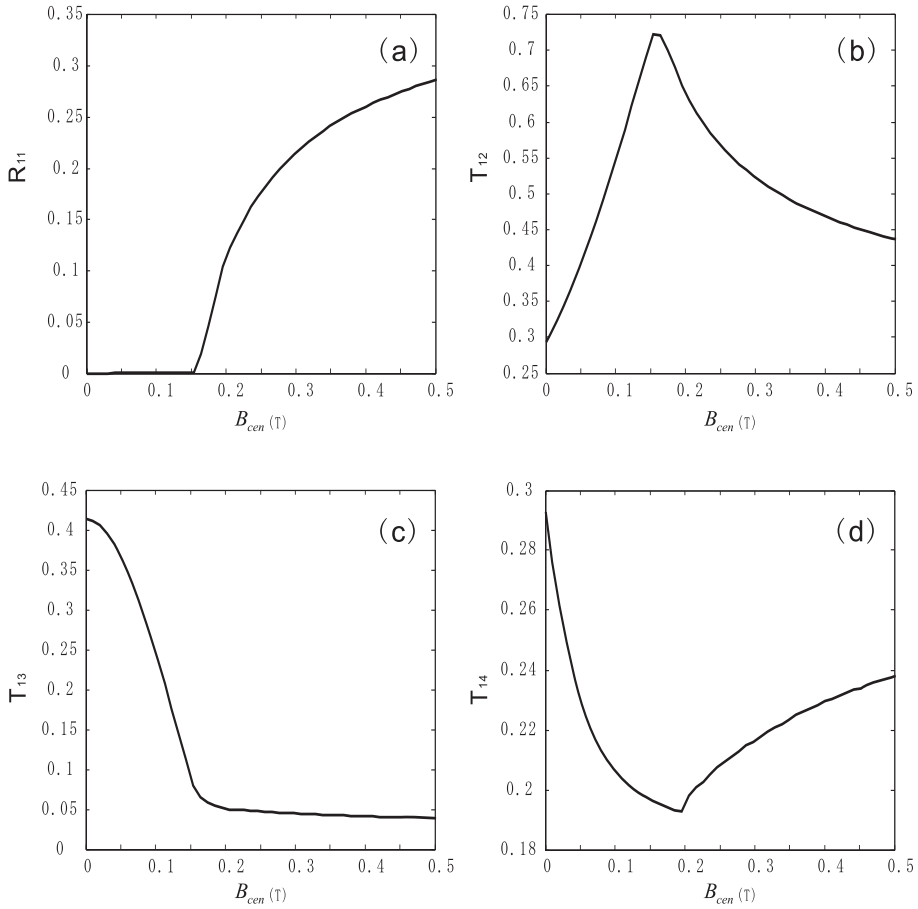

Fig. 4.3 The transport probability for a cylinder($R/W = 0.7$) placed at the center of the Hall cross. (a). reflection vs. B_{cen} (b). T_{12} vs. B_{cen} (c). T_{13} vs. B_{cen} (d). T_{14} vs. B_{cen}.

1. The reflection probability R_{11} becomes much smaller and it is zero at low field strength, this is reasonable since we only have a strong magnetic field in the junction area.
2. T_{12} looks very similar to the uniform field one, but note that we use B_{cen} here, and for a $R/W = 0.7$ cylinder, $B_{cen} = 2.78B_{av}$, so the actual T_{12} increases much faster than that in a uniform field. The peak of T_{12} occurs at about $B_{cen} = 0.154$ T ($B_{av} = 0.055$ T) here, compare to a uniform field value $B_c = 0.096$ T, this is the reason why the Hall resistance increases faster than that of a uniform field at intermediate field strength.
3. T_{13} also decreases when the field strength increases, but it never becomes zero, and it approaches a finite value about 0.04.
4. The situation for T_{14} has changed a lot from the uniform field one. From Fig. 2.9, we see that when T_{12} reaches its peak, T_{14} already becomes zero; but here, it does not go zero, and after that it even increases. This should be responsible for the suppression of the Hall resistance.

Since T_{13} and T_{14} are both larger than zero and even increase, the suppres-

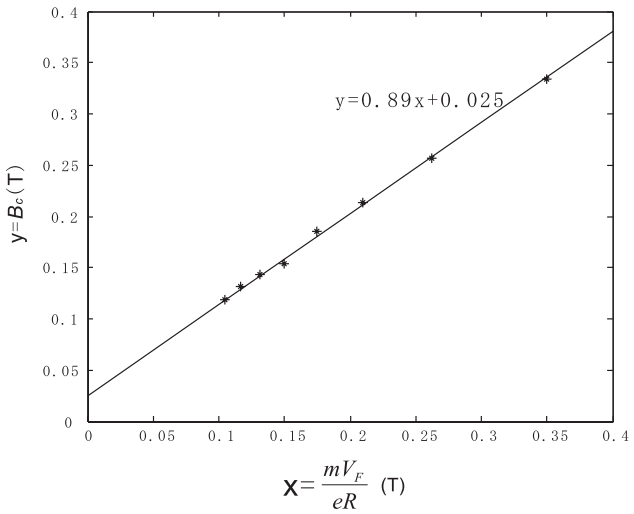

Fig. 4.4 The dependence of critical magnetic field B_c on the radius of the cylinder R. Stars: calculated value for the cylinders $R/W = 0.3, 0.4, ..., 1.0$; straight line: $y = 0.89x + 0.025$

sion of the Hall resistance will happen when T_{12} start to decrease, in other word, at the peak of T_{12}, we indicate this critical value as B_c. For cylinders having different radius R, from ref.[4], the relation between B_c and R can be expressed as:

$$B_c = a\frac{mV_F}{eR}, \text{ or, alternatively: } R = a\rho_c \tag{4.2}$$

where m is the effective mass of electrons, e the electron charge, V_F the fermi velocity, ρ_c the cyclotron radius, and a is a fitting parameter. We show this relation in Fig. 4.4, and we found that it is better to change Eq. (4.2) to $B_c = a\frac{mV_F}{eR} + b$, where b is an added fitting parameter. The straight line in Fig. 4.4 is for $a = 0.89$ and $b = 0.025$.

Why the transport probabilities change so much from those of the uniform field? To answer this question, we need to take a look how the electrons move inside the junction area. In Fig. 4.5, we show the typical electron trajectories when a $R/W = 0.7$ magnetized cylinder is placed at the center of the Hall cross, and let B_{cen} increases from 0.1 T to 0.5 T. These trajectories really give the answer we want. You can see, when B_{cen} is low, the magnetic field turns the electrons up, which will strengthen T_{12} and weaken T_{14}; then, the magnetic field far from the center area become more and more important, it turns the electrons down since it has a opposite field direction, which will strengthen T_{14}. This is the reason why T_{14} decreases at first, then increases, this is also the reason why T_{13} do not go to zero, and it causes the suppression of the Hall resistance. On the other hand, the bend resistance is very sensitive to the details of local magnetic field, the non-zero T_{13} and T_{14} cause it to increase to a positive value, and not saturate to zero as in the case of an uniform external field.

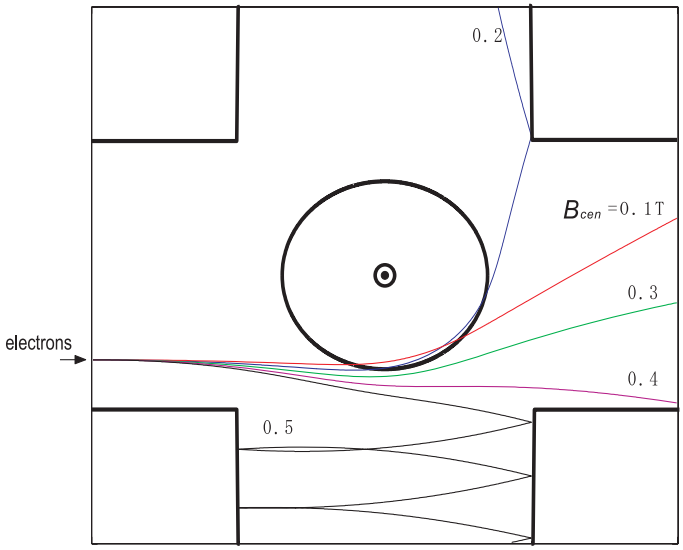

Fig. 4.5 Typical electron's trajectories for a $R/W = 0.7$ cylinder placed at the center of the Hall cross. The electrons are injected from the left side, and the field strength of the cylinder B_{cen} increases from 0.1 T to 0.5 T

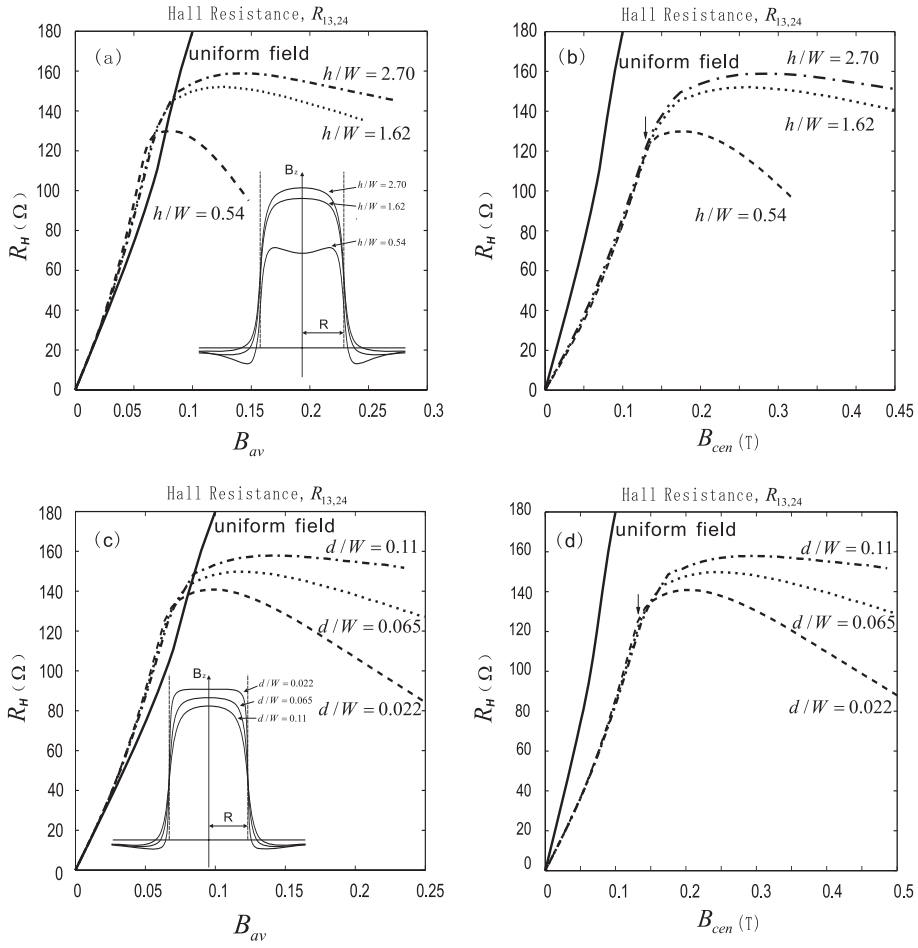

Fig. 4.6 The Hall resistance for a cylinder at center with different height h: (a) and (b), different distance d to 2DEG: (c) and (d). Inset of (a) and (d): the magnetic field profile for a cylinder at center with different h and d.

Now we turn to the situation that a cylinder is still placed at the center of the Hall cross, but with different height h, while keep all the other parameters the same. We show the Hall resistance as function of B_{av} and B_{cen} in Fig.4.6 (a) and (b). At low field strength, they are still the same to the uniform field one, then, still, increase faster followed by a suppression. Note that the cylinders are with same radius, so the Hall resistances should start to suppression at the same critical magnetic field B_c, this is true as the arrow indicated in Fig. 4.6(b). Before the suppression, they are almost the same line, but after that, the shorter cylinder suppress much stronger than

the longer one. To find an explanation, we just need to take a look what the differences in their magnetic field, as the inset of Fig. 4.6(a). They all experience a sign reverse of the field strength about $r = R$ the radius of the cylinder, this is the reason why they have the same B_c, but also note that the shorter cylinder has a stronger negative field strength, in other hand, a weaker positive field strength, so it will guide more electrons down, and less electrons up, this will strengthen the suppression.

Now we will vary the distance d between the magnetic cylinder and the 2DEG, while keep all the other parameters the same. The resulting Hall resistance is shown in Fig.4.6 (c) and (d). These results looks similar to the one from a cylinder with different height, but note the magnetic field profile which shown in the inset of (d), it's different to the one for change height. The $d/W = 0.022$ cylinder has the strongest suppression here, it also have the strongest positive and negative field strength, the positive field turn the electrons up and strengthen the Hall resistance, the negative field turn the electrons down and suppress the Hall resistance (Fig. 4.5), so we can conclude that the negative field has more important influence to the Hall resistance at large field strength since the result intend to suppress here.

Now we change another parameter, the electron density n_e for the 2DEG. The cylinder still put to the center of the Hall cross with all the other parameters the same, the resulting Hall resistance is shown in Fig. 4.7. It is

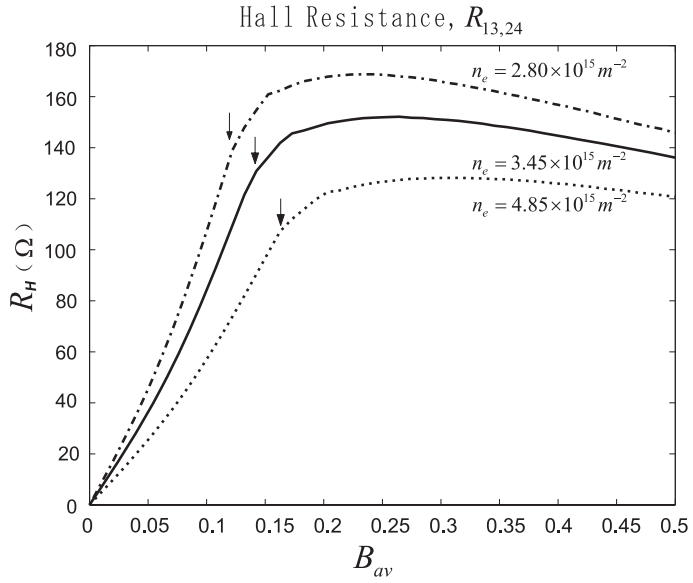

Fig. 4.7 Hall resistance for a cylinder at center, change the electron density. The arrow marked out where the Hall resistance start to suppress.

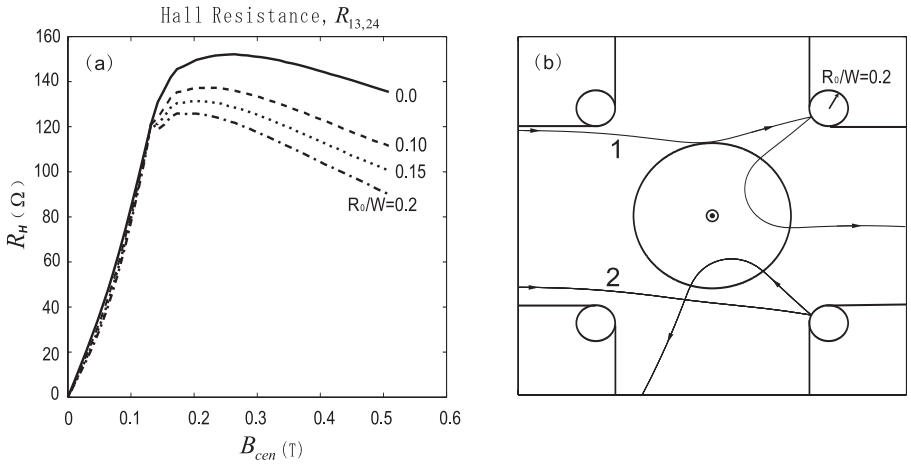

Fig. 4.8 A magnetized cylinder placed to the center of a Hall cross has rounded corner, the configuration of the system as shown in (b). (a) R_H vs. B_{cen}; (b) Typical electron trajectories for a Hall cross has rounded corner ($R_0/W = 0.2$) with a magnetized cylinder placed at the center.

obviously that the high electron density lead to a lower Hall resistance and a weaker suppression. It is easy to understand this behavior form the relation $V_F = \frac{\hbar\sqrt{2\pi n_e}}{m}$, the high electron density means high Fermi velocity, the high velocity electrons are hard to be guided by the magnetic field, this lower the Hall resistance and the suppression of it. The another thing need to notice is the critical value B_c of the suppression, from Eq. (4.2), B_c will change with V_F, as the arrows indicated in Fig. 4.7.

4.1.2 Effect of rounded corner of the Hall cross

If a Hall cross has rounded corner, the trajectories of electrons may become much more complicated when they experience reflect at the rounded corner. We show the Hall resistance for a cylinder at the center of a junction has rounded corner in Fig. 4.8(a). At low field strength, there is no noticeable change in the Hall resistance compare to a rectangle corner junction. But at high field strength, the rounded corner become important, it causes a small local peak when the Hall resistance start to suppress and a much stronger suppression. In Fig. 4.8(b) we plot typical electron trajectories which can explain this stronger suppression, the electron move along trajectory 1 reflected by the rounded corner and can not go up due to the guide of the magnetic field, this will decrease T_{12}; in contrast, the electron move along trajectory 2 also reflected by the rounded corner and still go down because the guide of the magnetic field, so T_{14} will not decrease, hence we got a stronger suppression.

4.1.3 One magnetized cylinder displaced from the center of the Hall cross

In this section we move the magnetized cylinder to different positions with respect to the center of the Hall cross. The results for a cylinder (all the parameters are keep the same) moving from the center to $x/W = -1.2$ along the x axis is shown in Fig.4.9 (a) and (b), the inset of (a) show the path of the cylinder. At low field strength, we still have that the Hall resistance is the same to the uniform field one, and still a faster increase at intermediate field followed by a quick suppression at high field. When the cylinder moved out from the junction region, the Hall resistance become more and more weak at the same B_{cen}, as shown in Fig. 4.9(b). This behavior is very similar to a cylinder at center which with small radius, as shown in Fig. 4.2(a), which imply that only the magnetic field inside the junction region has the most important influence to the Hall resistance. But note that the critical value B_c for the suppression, it almost unchanged when the cylinder moved out. Compare this to Fig. 4.2(c), which B_c change with R. So we can conclude that B_c is most depend on the geometry of the cylinder (actually the geometry of the magnetic field), but not depend on the field inside the junction region.

Now we use a smaller cylinder ($R/W = 0.5$, other parameters keep the same), so it can move inside the junction region, as shown in the inset of Fig. 4.9(d), the results also showed in Fig.4.9 (c) and (d). Still, the Hall resistance is completely determined by the average field in the junction area at low field strength. The critical value B_c is almost unchange since we do not change the radius of the cylinder. But for this cylinder move from down to up, the Hall resistance has been strengthen, this can be explained as: when the cylinder move up, it become close to lead 2 so it is easier to turn the electrons leave from that lead, which will increase our Hall resistance.

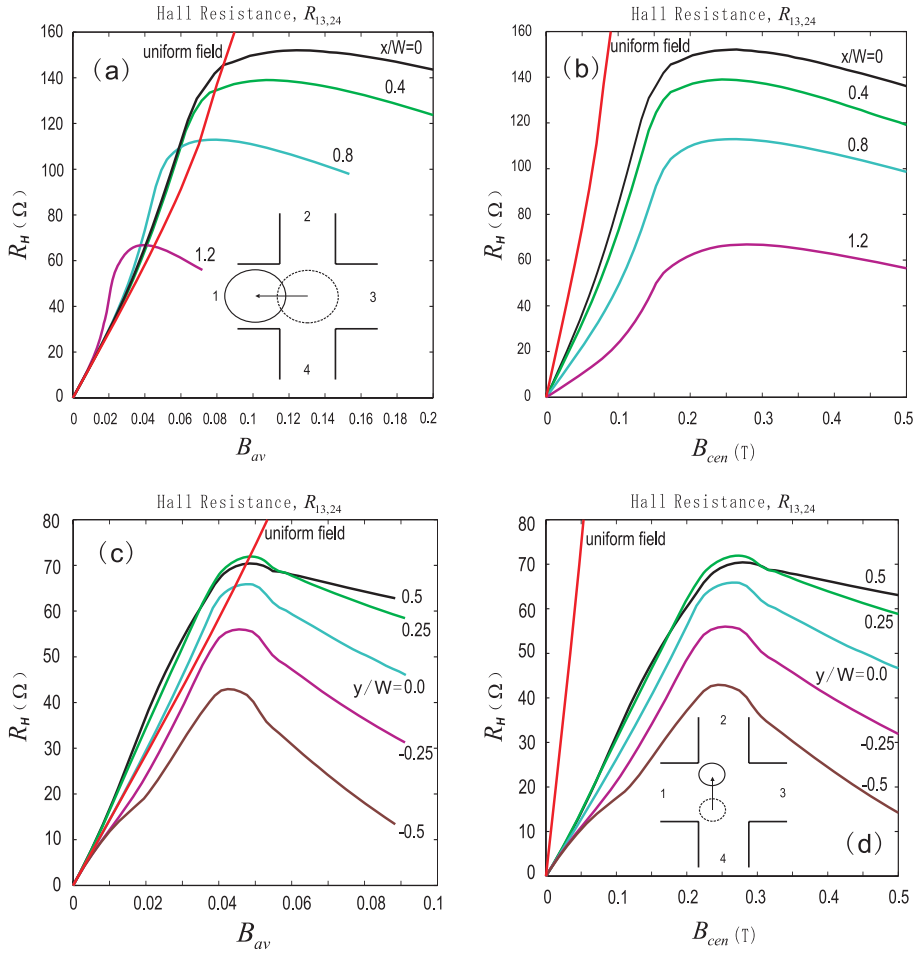

Fig. 4.9 Hall resistance for a cylinder displaced from the center. (a) and (b): the cylinder move along the x axis, the path is shown in the inset of (a). (c) and (d): the cylinder move at a line $x/W = -0.5$, the path is shown in the inset of (d).

4.2 SYMMETRY RELATED PROBLEMS

In the calculation above, we calculated the resistances for a four-terminal Hall cross using Eq. (2.20), now we want to discuss some symmetry problems related to this equation.

4.2.1 Symmetry for the current leads and voltage leads

The resistance $R_{mn,kl}$ for a Hall cross is measured when we have the current from lead m to lead n, and the voltage between lead k and l. If we reverse the current, from lean n to m, or the voltage, between l and k, it has been known that we have the following identities[10]:

$$R_{mn,kl} = -R_{nm,kl} = -R_{mn,lk}. \tag{4.3}$$

4.2.2 The reciprocity relation

The reciprocity relation[15] states that if we reverse the direction of the magnetic field but exchange the role of the current leads with the voltage leads, we will get the same resistance:

$$R_{mn,kl}(B) = R_{kl,mn}(-B). \tag{4.4}$$

Our results are in good agreement to this relation, and can be proved as follow. From Eq. (4.3), $R_{kl,mn}(-B) = R_{lk,nm}(-B)$, and from Eq. (2.20):

$$\begin{aligned} R_{lk,nm}(-B) &= N\frac{h}{2e^2}\frac{T_{nl}(-B)T_{mk}(-B) - T_{nk}(-B)T_{ml}(-B)}{D_{lm}(-B)}, \\ R_{mn,kl}(B) &= N\frac{h}{2e^2}\frac{T_{ln}(B)T_{km}(B) - T_{kn}(B)T_{lm}(B)}{D_{ml}(B)}. \end{aligned} \tag{4.5}$$

Have a look to this two equations, one can easily find that the only condition needed for $R_{mn,kl}(B) = R_{lk,nm}(-B)$ is $T(B)_{ij} = T(-B)_{ji}$. From our simulation, we find that $T(B)_{ij} \approx T(-B)_{ji}$. This can be explained if one refers to the trajectories of the electrons, as shown in Fig. 4.10. The left black arrow indicate an electron injected from lead 1, and we put two anti-magnetized cylinders to create the magnetic field, the electron leave from lead 4 due to the guide of the magnetic field; Then we reverse the magnetization of the cylinders, and injected an electrons from lead 4, at the exact position where the former one leave, with the same velocity and reverse the direction to the former one, as the red arrow indicated, then it will go exact the same trajectory and leave from lead 1. Actually for any magnetic field we will have the same situation, if an electron has been injected from lead i and leave from lead j, we can injected an electron from lead j, make it follow the same trajectory and leave from lead i. There is another thing need to notice that we inject electrons with an angular distribution $P(t) = \frac{1}{2}\cos(\theta)$, here the electron and its reversely move partner share the same trajectory but different injection angel, but we still have $T(B)_{ij} \approx T(-B)_{ji}$ since we injected so many electrons (10^6 as said before).

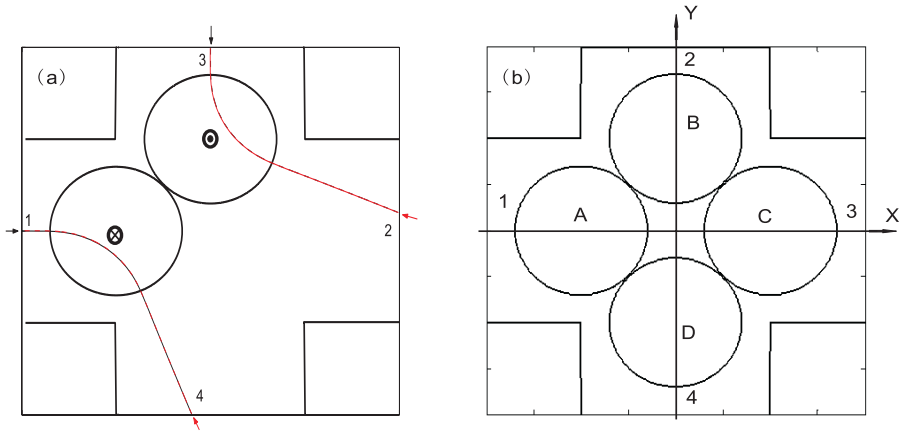

Fig. 4.10 (a) The typical electron trajectories for the reciprocity relation of the resistance. The black arrows and trajectories: the direction of magnetic field as shown in the figure; The red arrows and trajectories: the direction of magnetic field reversed. (b) Configuration of the system for the Hall resistance invariability.

4.2.3 The invariability of the Hall resistance for an axis symmetried magnetic field

It is found from our numerical simulation, if a magnetic field is symmetric with respect to one axis of the junction, the Hall resistance will be the same when put this magnetic field to different axis, but hold its distance to the center, as shown in Fig. 4.10(b): If we put an axis symmetried magnetic field to, for instance, one position of A, B, C and D, we will get the same Hall resistance. Or, alternatively, for an axis symmetried magnetic field, we have:

$$R_{13,24} = R_{42,13} = R_{24,31} = R_{31,42}. \tag{4.6}$$

This relation has been confirmed from the results of a cylinder, a box, a film or other more complicate systems. We can prove it as follow, from Eq. (4.3):

$$\begin{aligned} R_{13,24} &= R_{31,42}, \\ R_{42,13} &= R_{24,31}. \end{aligned} \tag{4.7}$$

Then we just need to prove $R_{13,24} = R_{42,13}$. Still, we need to find the electron trajectories which are responsible for this phenomenon.

In Fig. 4.11. We show these special trajectories. If we inject an electron from lead 4, it goes out from lead 3 due to the guide of the magnetic field, and because the magnetic field is symmetric to x axis, so we can inject an electron from lead 3, at the symmetry position to the first one and with reverse angel and velocity, this electron will leave from lead 2 with a symmetry trajectory.

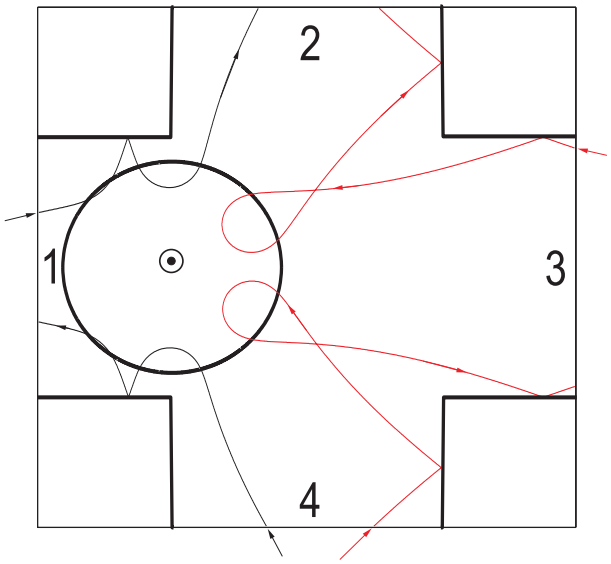

Fig. 4.11 The electron trajectories for the invariability of the Hall resistance when an axis symmetried magnetic field present, here we use a magnetized cylinder placed at $x/W = -1$, $y = 0$.

For every electron inject from lead 4 and leave from lead 3, we can find such a symmetry trajectory for electron injected from lead 3, and leave from lead 2. So as the same situation in reciprocity relation, we get $T_{43} \approx T_{32}$. The electrons go form lead 2 to lead 1 also have symmetry trajectories from lead 1 to lead 4, so we have $T_{21} \approx T_{14}$; for the same reason, we also have $T_{41} \approx T_{12}$, $T_{23} \approx T_{34}$ and $T_{31} \approx T_{13}$. Due to the symmetry magnetic field, we have another pair of transport probability T_{22} and T_{44} which are exact equal. From Landauer-Büttiker formula Eq. (2.20):

$$R_{13,24} = N\frac{h}{2e^2}\frac{T_{21}T_{43} - T_{23}T_{41}}{D_{14}},$$
$$R_{42,13} = N\frac{h}{2e^2}\frac{T_{14}T_{32} - T_{12}T_{34}}{D_{43}}. \tag{4.8}$$

substitute all the equal relations which mentioned above to these two equations, one will find:

$$R_{13,24} = R_{42,13}. \tag{4.9}$$

In Fig. 4.12, we compare the Hall resistance of a magnetic field which is symmetric to one axis to that of a magnetic field do not symmetric to any axis, it is in good agreement to our calculation here.

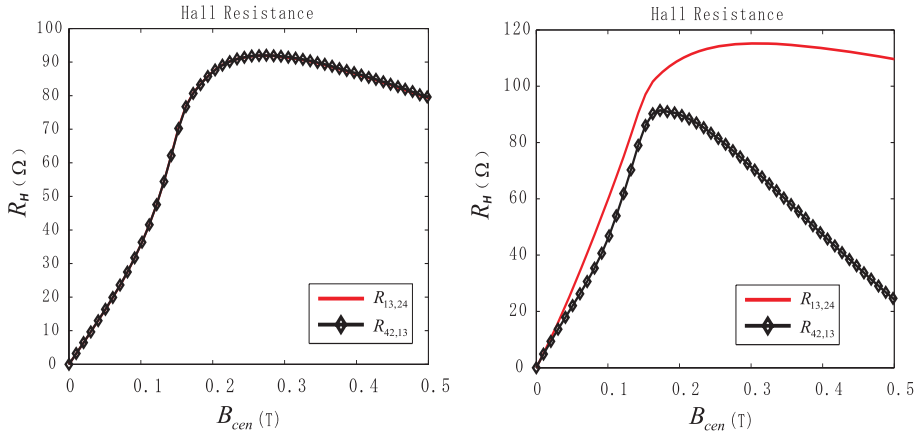

Fig. 4.12 (a) Hall resistance for a cylinder at $x/W = -1$, $y = 0$, which is symmetric to x axis; (b) Hall resistance for the cylinder move to $x/W = -0.5$, $y/W = 0.5$, which do not symmetric to any axis.

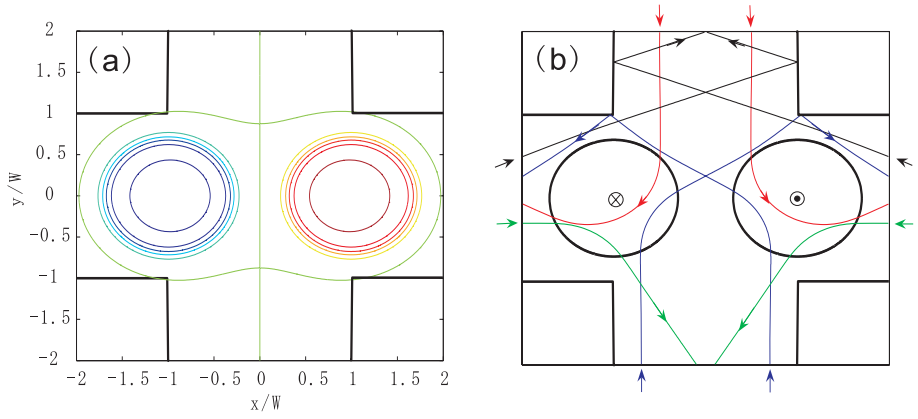

Fig. 4.13 (a) Example for anti-symmetried magnetic field. (b) Typical electron trajectories in a Hall cross with anti-symmetried magnetic field.

4.2.4 Zero Hall resistance for an axis anti-symmetried magnetic field

If the magnetic field is anti-symmetric with respect to one axis as shown in the Fig. 4.13(a), the Hall resistance will always be zero. From the electron trajectories in Fig. 4.13(b), we can easily find that: $T_{21} = T_{23}$, $T_{41} = T_{43}$, $T_{14} = T_{34}$ and $T_{12} = T_{32}$, substitute these relations into Eq. (4.8) results into:

$$R_{13,24} = R_{42,13} = 0 \tag{4.10}$$

4.3 TWO CYLINDERS

Two cylinders with radius $R/W = 0.7$:

The typical magnetic field for 2 identical cylinders with radius $R/W = 0.7$ and parallel magnetization is shown in Fig. 4.14(a). We hold one cylinder in position $(x_1/W, y_1/W) = (-1, 0)$, put another cylinder to different positions: $(x_2/W, y_2/W) = (0, -1)$, $(1, 0)$ and $(0, 1)$ (see the inset of Fig. 4.14(c)). The results for the Hall and bend resistance are shown in Fig.4.14 (c) and (d). At low field strength, the Hall resistance still simply depend on the average field in the junction; But when the field strength increases, the Hall resistance becomes very sensitive to the position of the second cylinder. The more we place it towards lead 2, the smaller the the Hall resistance will be. This is different from the one cylinder case as shown in Fig.4.9 (c) and (d), where the Hall resistance was found to increase when we put the cylinder towards lead 2. In order to explain this different behavior, I plot typical electron trajectories in Fig. 4.14(b). When we have the second cylinder at $(x_2/W, y_2/W) = (0, -1)$, the trajectories of electrons injected from the left side at position a and b is very similar to the situation that there is no second cylinder; but the electron injected from position c is reflected by the second cylinder. For comparison, I removed the second cylinder and injected an electron from the same position, as indicated by the red trajectory, the electron will now leave the cross through lead 4 which is the most important reason for the suppression of the Hall resistance. So, the second cylinder prevents the electrons to leave through lead 4 and this strongly decreases the suppression of the Hall resistance. On the other hand, if we put the second cylinder towards lead 2 as $(x_2/W, y_2/W) = (0, 1)$, it can not prevent the electrons to leave from lead 4, and it even helps them, since it will increase the negative field strength at lower region and guide more electrons towards lead 4.

Then I have the second cylinder be oppositely magnetized, and keep all the other parameters the same. I show the Hall and bend resistance as function of B_{cen} (B_{av} is zero here) in Fig.4.14 (e) and (f). The Hall resistance for the second cylinder at $(1, 0)$ is zero, since its magnetic field is anti-symmetric to the y axis. The Hall resistance for the second cylinder at $(0, -1)$ is the reverse number to that of the second cylinder at $(0, 1)$, this can be prover from the reciprocity relation. Note that here the Hall resistance does not only depend on the average field B_{av} in the junction even at low field strength, it does not remain zero in spite of B_{av} which is always be zero, this will be checked further.

Two cylinders with radius $R/W = 0.3$:

Then I use two smaller cylinders ($R/W = 0.3$, other parameters keep the same), they can be put both inside the junction area. We place one cylinder at the center and put the other cylinder at a fixed distance from the center, then vary the angular position, as shown in the inset of Fig. 4.15(b). In Fig. 4.15(a) and (b), I show the contour plot of typical magnetic field profile for these two cylinders with parallel or anti-parallel magnetization. And in Fig. 4.15(c), (d), (e) and (f) I show the Hall and bend resistance for the cylinders which are parallel or anti-parallel magnetized.

If these two cylinders are anti-parallel magnetized, the average magnetic field B_{av} inside the junction is very weak, but we still find a significant Hall resistance and if the second cylinder is placed at an angel θ rotated from the axis, the Hall resistance will differ from that of the uniform field case even at very low field strength, as indicated by the blue and green curves in Fig.4.15 (e).

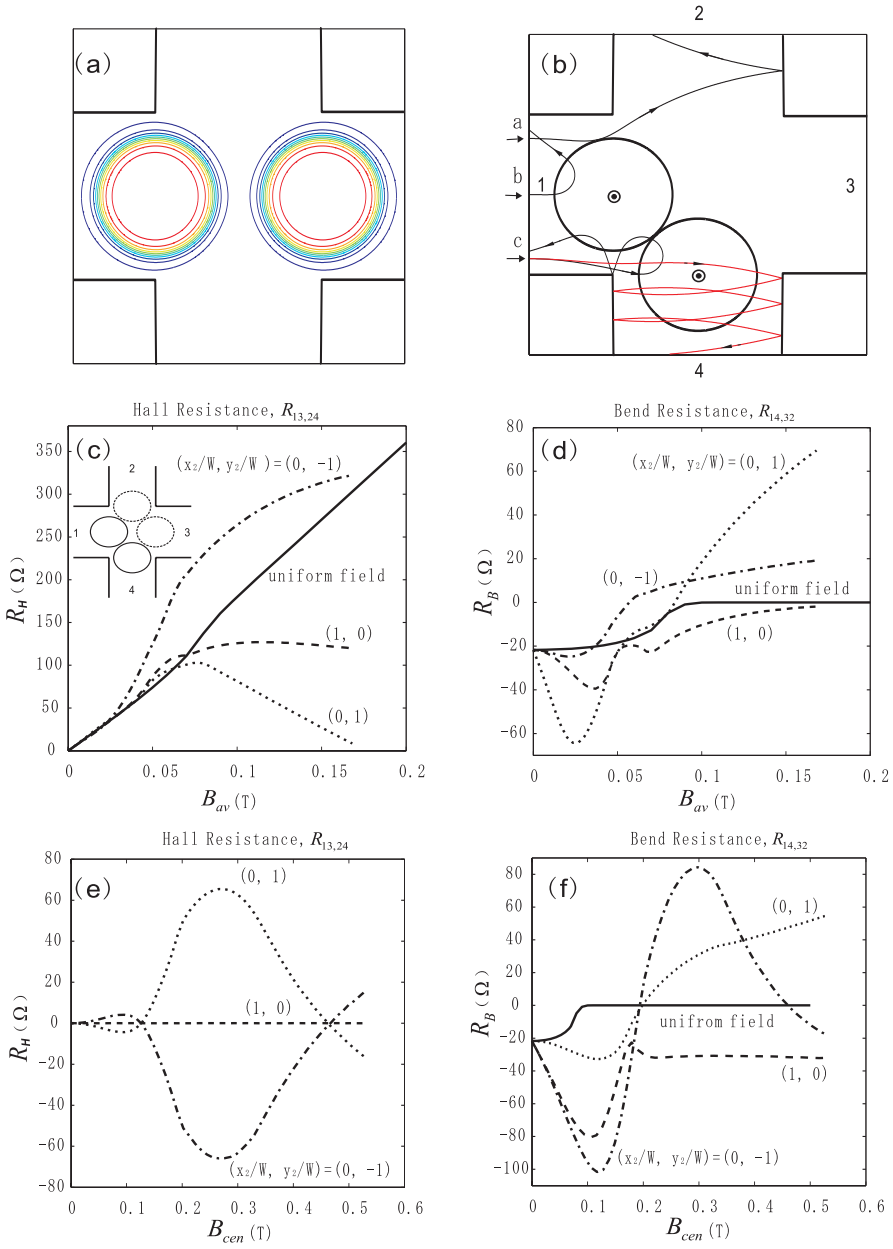

Fig. 4.14 Two identical cylinders with radius $R/W = 0.7$, other parameters are keep the same. (a) Contour plot of the magnetic field when the cylinders are parallel magnetized, for the anti-parallel magnetized cylinders see Fig. 4.13(a); (b) Some typical electron trajectories; (c) and (d) the Hall and bend resistance for a cylinder hold at $(x_1/W, y_1/W) = (-1, 0)$, and the other cylinder is put at $(x_2/W, y_2/W) = (0, -1)$, $(1, 0)$ and $(0, 1)$ (see the inset of (c)); (e) and (f) the Hall and bend resistance for the second cylinder is anti-parallel magnetized, other parameters keep the same with those in (c) and (d).

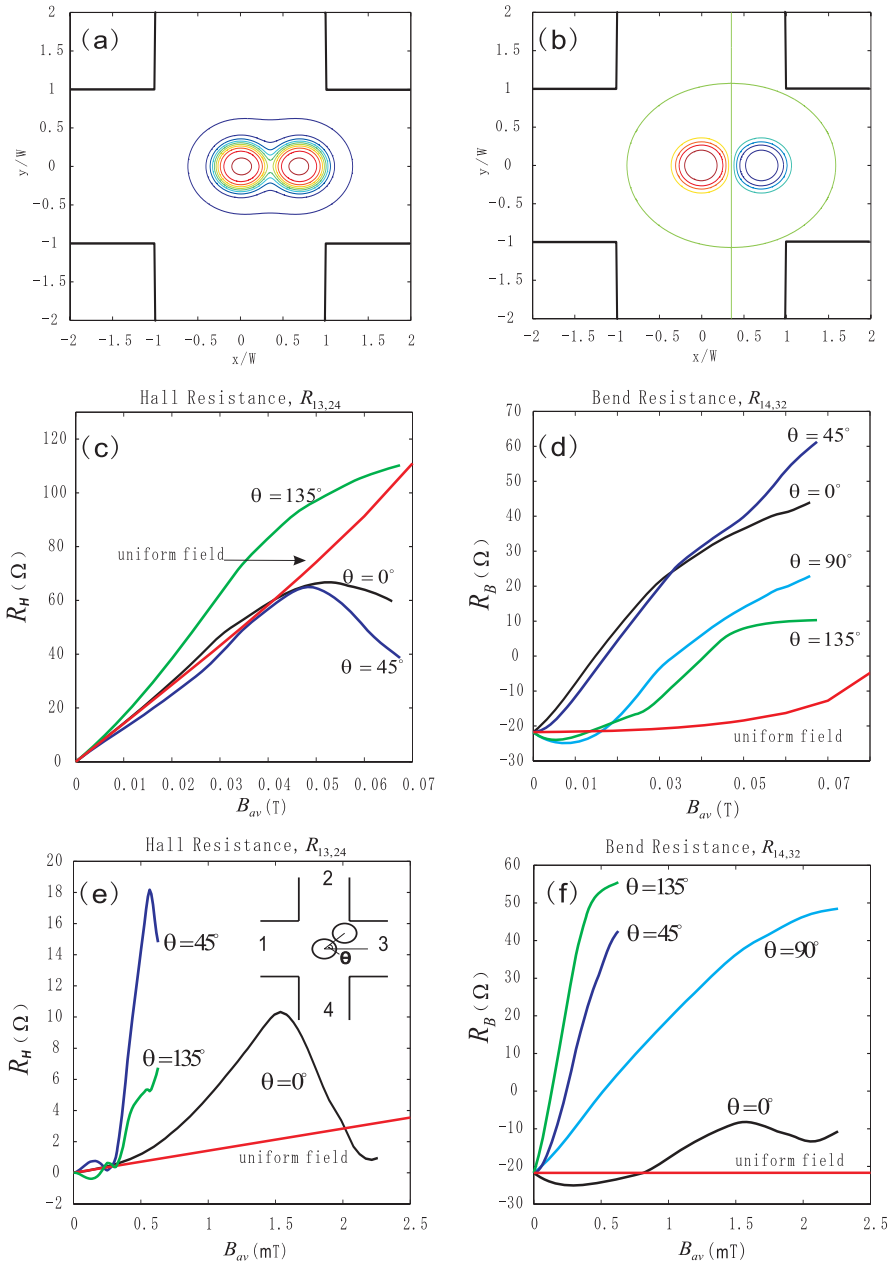

Fig. 4.15 Two identical cylinders with radius $R/W = 0.3$, other parameters are keep the same. The first cylinder placed at the center, the second one placed at fixed distance to the center $\rho/W = 0.7$, and has a rotation angel θ to the x axis, see the inset of (e). (a) and (b) Contour plot of typical magnetic field profile for the cylinders are parallel or anti-parallel magnetized; (c) and (d) the Hall and bend resistance for the two cylinders have parallel magnetization; (e) and (f) the Hall and bend resistance for the cylinders are anti-parallel magnetized.

5

Hall bar response in the presence of magnetized boxes and thin films

5.1 BOXES

The situation for magnetized boxes are very similar to magnetized cylinders, since they have very similar magnetic field profiles, except with one main difference: the magnetic field profile for boxes is not a circular symmetric one, see Fig. 5.2(a). We indicate the length of the sides of a box by w_x and w_y, as shown in Fig. 3.1, and keep all the other parameters the same as for cylinders. In Fig.5.2 (c) and (d) we show the Hall and bend resistances for a box placed in the center with different w_y as function of B_{av}, Fig.4.2 (a) and (b) are the results for a cylinder at the center of the Hall cross with different radius. They have very similar behavior: At low field strength, the hall resistance is still completely determined by the average field in the junction; then it increases faster than that for a uniform field at intermediate field strength; and at high field strength the Hall resistance is reduced.

We want to know if the relation $B_c = a\frac{mV_F}{eR}$ (Eq. (4.2)) still holds here. We need to replace R by $\sqrt{\frac{wx \cdot wy}{\pi}}$ in Eq. (4.2) since there is no R for a box. In Fig. 5.2(b) we plot this relation for $w_x/W = 1.6$, $w_y/W = 0.4, 0.8, 1.2, 1.6$ boxes, and the best fit is found to be $a = 1.10$, as the straight line indicates. We try to apply this relation for the uniform external field case, since the effective area for the Hall resistance is only the junction area, we can roughly take it as a $w_x = w_y = 2W$ box, which yields a critical value $B_c = 0.102$ T, and is 6.3% larger than the real one $B_c = 0.096$ T.

5.2 THIN FILMS

The film we model as a thin box and for our numerical calculations we took: $w_x/W = w_y/W = 1.5$ as the side length, $t/W = 0.16$, the thickness of the film, and all the other parameters are the same as for the previous case of cylinders.

The typical magnetic field profile for such a thin film is shown in Fig. 3.3. Note that it is similar to two anti parallel magnetized narrow boxes put together, but the maximal field strength is much smaller than for a box or a cylinder with the same magnetization, and thus its average field B_{av} is also low. In Fig. 5.3 we show the Hall and bend resistances for thin films put at different positions. For a single film we put it to the position as shown in the inset of Fig. 5.3(a), and for 2 films they are placed at opposite positions as shown in the inset of Fig. 5.3(c). Notice that the Hall resistance is comparable to the uniform field one. For two films with the same direction of magnetization, as shown in the inset of Fig. 5.3(e), the magnetic field is anti-symmetric with respect to the y axis (see Fig. 5.1), the average field B_{av} is zero, and therefore we use B_{max} (the maximal field strength underneath the film) here. The Hall resistance will always be zero for an anti-symmetried magnetic field as discussed in section **4.2**. On the other hand, the bend resistance is much sensitive to the details of the magnetic field and is found to vary with the strength of the magnetic field.

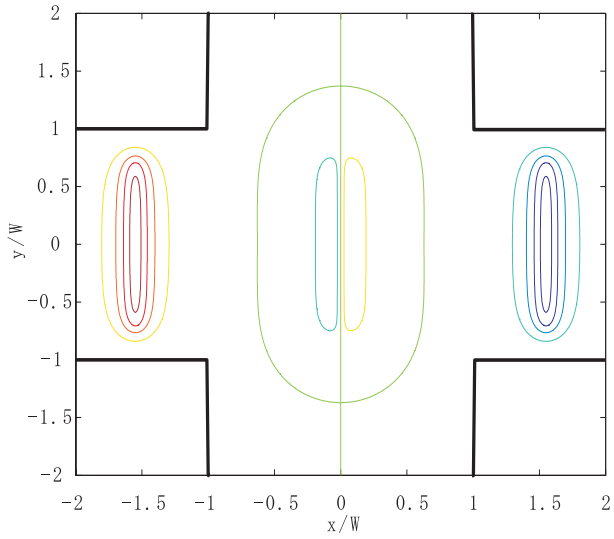

Fig. 5.1 Contour plot for the magnetic field profile of two parallel magnetized films (see the inset of Fig.5.3 (e)).

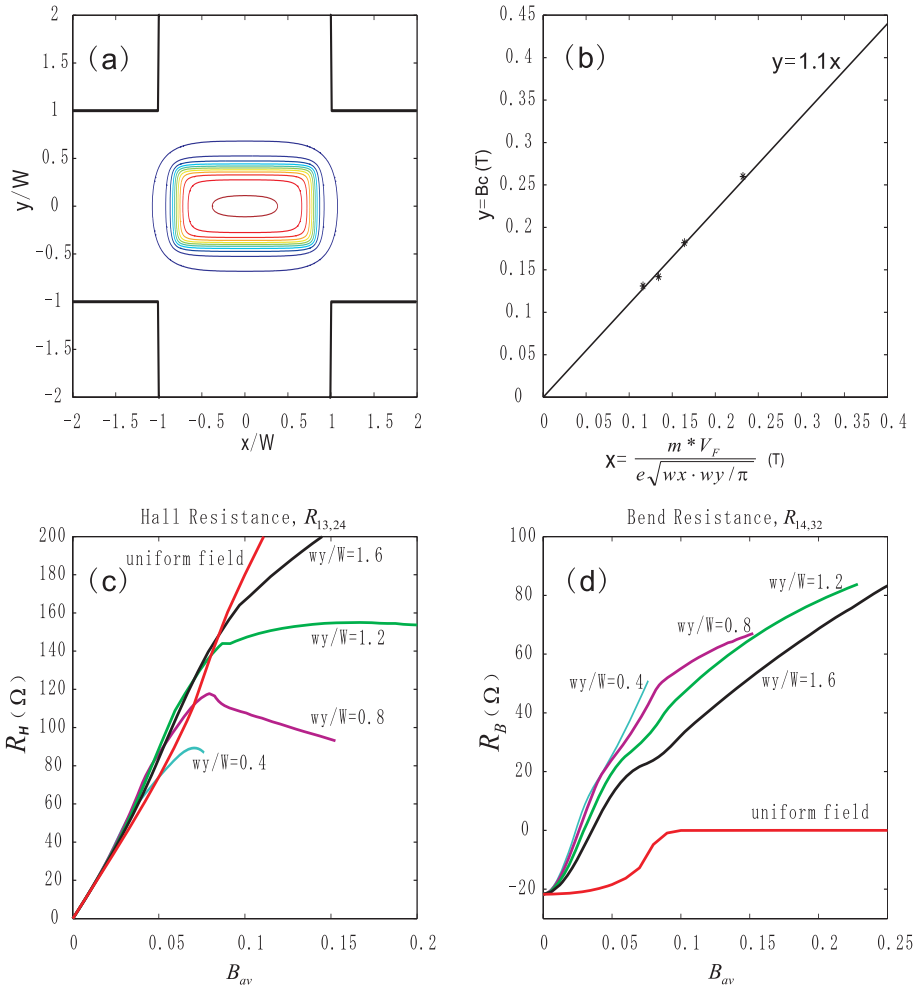

Fig. 5.2 (a) The contour plot of magnetic field profile for a box ($w_x/W = 1.6, w_y/W = 0.8$, other in default) at center. (b) The relation between the size of the box and the critical value B_c. (c) and (d) Hall and bend resistance for boxes: $w_x/W = 1.6, w_y/W = 0.4, 0.8, 1.2, 1.6$, other parameters keep the same.

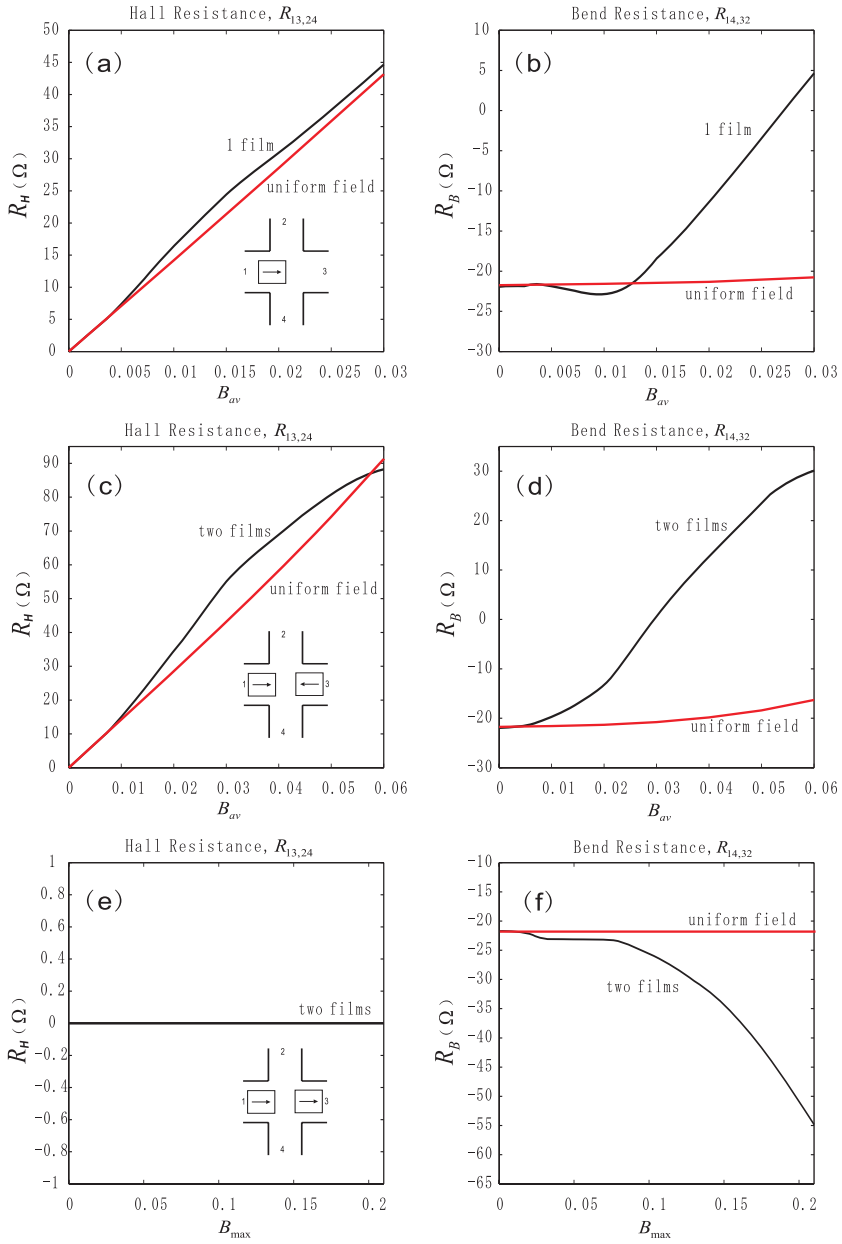

Fig. 5.3 The Hall and bend resistance for thin films ($w_x/W = w_y/W = 1.5$ and $t/W = 0.16$, the other parameters keep the same) placed at different positions. (a) and (b) Single film placed at $(x/W = -0.75, y/W = 0)$, see the inset of (a); (c) and (d) Two films opposite placed at $(x/W = -0.8, y/W = 0)$ and $(x/W = 0.8, y/W = 0)$ respectively, see the inset of (c); (e) and (f) Two films placed at the same positions as in (c) and (d), but with parallel magnetization, see the inset of (e);

6

Conclusion

In this thesis we investigated the Hall and bend resistance for a micron-sized Hall bar in the ballistic regime. The Hall bar was studied in the presence of a strong inhomogeneous magnetic field. Such fields were the result of uniform magnetized ferromagnetic dots that are placed in the junction region. The transport probabilities of the electrons that are scattered in the Hall bar are obtained by using the semiclassical billiard model. The Hall and bend resistances follow from the Landauer-Büttiker formula.

First, we studied the scenario that there is only one magnetized cylinder in the junction region. The magnetic field underneath the magnetized cylinder has a step-like profile: strong field strength in a small area below the cylinder and a much weaker field strength with opposite direction outside this area. In the low field regime, the Hall resistance is completely determined by the average field in the junction. At intermediate field, the Hall resistance increases faster than the result expected from the average field. When further increasing the magnetization, the Hall resistance is suppressed. This suppression is due to the sign reversal of the magnetic field profile. At high field strength, the electrons will be more influenced by the field outside the center where the field has the opposite sign resulting in a suppression of the Hall resistance. The critical value where the Hall resistance starts to be suppressed depends mainly on the radius of the cylinder (actually, the geometry of the magnetic field profile) and the Fermi velocity of the electrons. If we put a cylinder with fixed radius at different positions, this critical value for suppression is only slightly changed. The other parameters of the cylinder will not influence the critical value, but influences the strength of the suppression. The effect of a Hall bar with rounded corner was also investigated, which will yield a stronger

suppression due to special electron trajectories that experience reflection at the rounded corner.

Then we studied the situation for two cylinders in the region. If these two cylinders are parallel magnetized, at high field regime, the Hall resistance is sensitive to the position of the cylinders; at low field regime, it still depends only on the average field in the junction. But if these two cylinders are anti-parallel magnetized, the Hall resistance becomes very sensitive to the position of the cylinders at any field strength.

Our study shows that the Hall bar can be used as a very sensitive sensor to probe the direction of the magnetization of the ferromagnetic dots (or cylinders). This can also be used to investigate the magnetic interaction between e.g. two ferromagnetic cylinders, a topic of high current interest in view of the increased density of magnetic storage.

We also studied the situation for magnetized boxes and thin films in the Hall bar region. We found that the Hall resistance shows a similar behavior as that found for cylinders.

We found two symmetry related problems from our simulation: First, if a magnetic field profile is symmetric with respect to one axis of the Hall cross, the Hall resistance will become invariant when we move this magnetic field profile towards different leads of the Hall cross but keep its distance to the center the same; second, if a magnetic field profile is anti-symmetric to one axis, the Hall resistance will always be zero.

At the same time we also investigate the bend resistance which was found to be a much more sensitive function of the exact shape and position of the magnetic field profile. The interpretation of those results are less straight forward.

References

1. E. Hall, Am. J. Math. **II**, 287 (1879).

2. For a review see, e.g., T. Chakraborty and P. Pietilä nen, *The Quantum Hall Effects* (Springer, Berlin, 1995).

3. A. Oral, S. J. Bending and M. Henini, Appl. Phys. Lett. **69**, 1324 (1996).

4. K. S. Novoselov, A. K. Geim, S. V. Dubonos, Y. G. Cornelissens, F. M. Peeters, and J. C. Maan, Phys. Rev. B **65**, 233312 (2002).

5. A.K.Geim, S. V. Dubonos, J. G. S. Lok, I. V. Grigorieva, J. C. Maan, L. Theil Hansen and P. E. Lindelof, Appl. Phys. Lett. **71**, 2379 (1997).

6. Supriyo Datta, *Electronic Transport in Mesoscopic Systems* (Cambridge University Press, Cambridge, 1999).

7. B. J. van Wees, H. van Houten, C. W. J. Beenakker, J. G. Williamson, L. P. Kouwenhoven and D. van der Marel and C. T. Foxon, Phys. Rev. Lett. **60**, 848 (1988).

8. R. Landauer, IBM J. Res. Dev. **1**, 233 (1957).

9. M. J. Kelly, *Low-dimensional semiconductors* (Oxford University Press, New York, 1995).

10. M. Büttiker, Phys. Rev. Lett. **57**, 1761 (1986).

11. K. L. Shepard, M. L. Roukes, and B. P. Van der Gaag, Phys. Rev. Lett. **68**, 2660 (1992)

12. C. W. J. Beenakker and H. van Houten, Phys. Rev. Lett. **63** 1857 (1989).

13. J. D. Jackson, *Classical Electrodynamics* (3ed, John Wiley & Sons Press, New York, 1998) Page **197** and **101**.

14. F. M. Peeters and X. Q. Li, Appl. Phys. Lett. **72**, 572 (1998).

15. L. J. van der Pauw, Philips Res. Rep. **13**, 1 (1958).